Aeroacoustic Validation of Installed Low Noise Propulsion for NASA's N+2 Supersonic Airliner

James Bridges[1]

NASA Glenn Research Center, Cleveland, OH 44135

An aeroacoustic test was conducted at NASA Glenn Research Center on an integrated propulsion system designed to meet noise regulations of ICAO Chapter 4 with 10EPNdB cumulative margin. The test had two objectives: to demonstrate that the design meets the noise goal and to validate the noise prediction tools used during the design process. Variations in the propulsion system design and its installation were tested and the results compared against predictions. Far-field microphones measured the acoustic spectral directivity, which was transformed to full scale and used to compute noise certification levels. Phased array measurements confirmed that the shielding of the installation model adequately simulated the full aircraft and provided data for validating RANS-based noise prediction tools. Particle image velocimetry confirmed that the flow field around the nozzle on the jet rig mimicked that of the full aircraft and produced flow data to validate the RANS solutions used in the noise predictions. The far-field acoustic measurements confirmed the empirical predictions for the noise. Results provided here detail the steps taken to ensure accuracy of the measurements and give insights into the physics of exhaust noise from installed propulsion systems in future supersonic vehicles.

Nomenclature

h_E	standoff height of planform from nozzle lipline
k	flight exponent
Ma	acoustic Mach Number; jet velocity divided by ambient speed of sound
M_{flight}	Ambient Mach number or flight speed
U	mean velocity
x_E	length of planform from nozzle to trailing edge
b	denotes bypass stream
c	denotes core stream
t	denotes tertiary stream

I. Introduction

NASA's Commercial Supersonic Technology Project formulated a milestone, referred to as a Technical Challenge, to design a low-noise propulsion system on a low-boom aircraft that could meet the airport noise regulations of today with enough margin to justify further development. Work on the Low Noise Propulsion Tech Challenge is documented elsewhere[1] in this conference. The study was limited to a fixed low-boom airframe, but included exploration of different engine architectures, nozzle systems, the acoustic effect of installation, and airport operations. The work included development of noise prediction methods, from extensions of empirical noise models, development of predictions using Reynolds-Averaged Navier-Stokes (RANS) simulations, and explorations of Large Eddy Simulations (LES). The work was performed over many years with academic investigators, industry teams, and NASA researchers. The acoustic performance of low-noise nozzle concepts was captured in empirical models for use in systems studies. System-level design work led to a selection of engine cycles and nozzles that, when mounted on a conceptual vehicle, would meet the success criterion on noise. These successful cycle/nozzle designs were selected for rig testing in an acoustic test to validate these designs. The propulsion system exhaust nozzles, as installed on the conceptual aircraft, had to be represented in model scale hardware, the far-field sound measured and transformed to full-scale flight as the aircraft would operate during certification, and the validity of the measurements and the fidelity

---

[1]Research Engineer, Acoustics Branch, AIAA Associate Fellow

of the model had to be demonstrated. The present report summarizes this validation test, internally referred to as the *JSI16* (*Jet-Surface Interaction 2016*) test, which was conducted at NASA Glenn's Aero-Acoustic Propulsion Lab in late summer 2016.

Prior testing of inverted velocity profile (IVP) nozzles and three-separate-stream nozzles created empirical jet noise models for isolated nozzles. These models were combined with system-level engine models to determine optimum cycles/nozzles that would give the best flight range with acceptable noise at the airport. The result was a large matrix of engines and predicted noise levels, reflecting the trades one would make in a large system optimization exercise. Several of these engines, representing optimal solutions for different priorities, were selected for final validation of the empirical noise models. These nozzles were tested in isolation during the *Iso16* test conducted in February 2016.

In spring 2015, a test program, called *JSI1044*, documented[2] the use of a flat-panel planform representation of the Lockheed Martin 1044 (*LM1044*) supersonic airliner concept in tests without simulated flight. This test taught critical lessons how to represent aircraft bodies in aeroacoustic tests. It also provided data allowing extension of empirical jet-surface interaction (JSI) models to more complicated situations involving finite span surfaces[3] and multiple-stream nozzles[4]. The only remaining feature to the JSI modeling not accounted for was the effect of flight on the noise.

The *JSI16* test married the best nozzle/engine combinations from the *Iso16* test with a *LM1044* planform model, derived from the *JSI1044* test, that could be used in a flight stream. The flow conditions used in this test came from NASA simulations of a three-stream engine using Numerical Propulsion Simulation System (NPSS)[5]. The predicted engine performance for a large range of engine designs was applied to an aerodynamic vehicle model of the *LM1044* aircraft to predict range for the aircraft. In that analysis, predictions of lateral EPNL from the jet noise component were plotted against predicted range. A subset of the study is shown in Figure 1. With some assumptions about other aircraft noise components, a surrogate EPNL level of 93.3 EPNdB was established that served as the maximum sound level that the aircraft could make at the lateral certification observer and still certify at Chapter 4 with a 10EPNdB cumulative margin. This is given as a dashed line in Figure 1. Eight engine designs, shown in the figure by the open symbols, were selected that met the goal either at 100% throttle or with some amount of reduction, such as would be achieved using a programmed lapse rate (PLR). The selections were made to include several types of nozzles and to maximize the predicted range for each of these types.

This report documents the test objectives, facility, model configurations and flow conditions tested, and the instrumentation systems used.
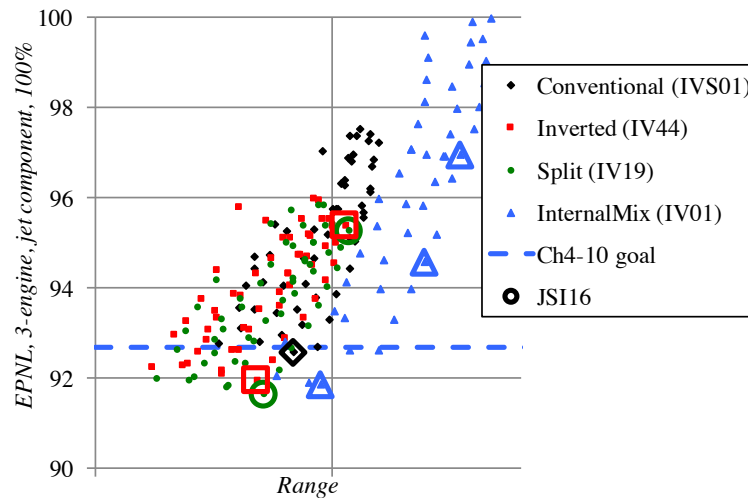
Figure 1. Chart showing predicted airport noise vs aircraft range for LM1044 aircraft with various propulsion systems. Different colors indicate different nozzles (description below) and open symbols highlight the propulsion designs validated in the JSI16 test.

II.   Test Objectives

1. Validate representation of LM1044 by test hardware.
    a. Confirm that test model planform has adequate coverage to reproduce the shielding of the aircraft.
    b. Confirm that rig/planform mimics the ambient flow of actual aircraft around the nacelle/nozzle.
2. Validate that installed propulsion meets noise goal.
3. Acquire database for flight effect on the acoustics of jet-surface interaction.
4. Validate design sensitivities as predicted by empirical models.
    a. Engine parameters (engine cycle/nozzle type)
    b. Planform (deck length, x_E)
    c. Flight speed (M_{flight})
    d. Propulsion location (center/outboard) and azimuthal noise dependence
5. Acquire flow-field surveys of mean and turbulent velocities
    a. Document impact of surface on jet plume for CFD validation

III.   Facility

The test was conducted in the NASA Glenn Research Center Aero-Acoustic Propulsion Laboratory (AAPL), shown in Figure 2. The AAPL is a 65-foot radius anechoic geodesic hemispherical dome. Acoustic wedges cover the walls of the dome and approximately half of the floor area. The AAPL was acoustically clean for all acoustic test runs, with acoustic wedges on the front and microphone sides of all rigs and on the floor of the facility. No untreated objects were within 40 feet of the jet exit and within view of the jet nozzle. The ambient temperature, pressure, and relative humidity were recorded within the dome during each data acquisition and used to transform the data to that of a flight on a standard day.

The Nozzle Aeroacoustic Test Rig (NATR) is contained in the AAPL. The NATR provides the flight stream for the jet rig. The NATR ductwork was acoustically lined on both the inside and outside and consisted of an annular ejector system connected to a plenum followed by the transition section which was a long-radius, low-beta venturi nozzle. This flow was exhausted through a 53-inch diameter nozzle that formed a free jet to simulate the effects of forward flight on the test article. The centerline of the free jet was 10 feet above the floor. This arrangement could produce Mach numbers in the free jet up to 0.35. An acoustically treated wall separated the NATR from the section of the building which did not have acoustic treatment on the floor, preventing unwanted reflections from the both the untreated floor area and adjacent test equipment.

A turbofan engine simulator, the High Flow Jet Exit Rig (HFJER), was located at the downstream end of the NATR. Compressed air was delivered from centralized compressors to the test article through a system of manifolds, heaters, flow measuring ventures, control valves, and flow conditioners. All air streams were preheated using a mixed flow head exchanger before being split into three streams, independently metered and pressure-controlled, and directed to co-annular settling chambers in the rig. The innermost air stream was further heated using a natural gas combustor up to 1200°F. The second and third air streams were independently controlled for pressure, but not for temperature. The combined mass flow of the three streams was 30 lbm/sec.

The rig was instrumented to record total temperature, total pressure, and static pressure at a charging station on all streams. In addition, mass flowrates were recorded using flow venturi. Ambient conditions were recorded simultaneously with the acoustic and flow measurements. Relative humidity and temperature were recorded both at 10' above the floor near the NATR and at the top-most region of the overhead microphone array, located roughly 60' above the floor. The 60' temperature was used in corrected the acoustic data, but the measurements at 10' and 60' could be checked to be sure there were negligible temperature gradients that would complicate the corrections. Ambient pressure was recorded in a sheltered location within the dome.

The research instrumentation consisted of the far-field microphone array, a 48-microphone phased array, and the particle image velocimetry (PIV) system, as seen in Figure 2. These measurement systems were operated individually in succession (not simultaneously). Each system requires the facility to be configured for its needs: the overhead array requires the entire dome test area to be covered in acoustic wedges. The phased array required a scaffold to position it and minimal acoustic wedges to reduce reflection directly behind the model. The PIV system required a large translating optical bench ('Big Blue'), no acoustic wedges, and black optical backdrops.

Figure 2 Instrumentation systems, clockwise from left: far-field acoustic array, Array48 phased array, PIV system.

IV.   Model Hardware

Model configurations were described by the rig, nozzle, planform subsystems, and the support structure to hold them together. This section catalogues the hardware subsystems.

A. Rig hardware

The HFJER was augmented by a rotating spool piece that served as a mount point for the planform support. The mount point on the outer layer of the rotating spool piece could be spun about the jet rig axis to allow azimuthal positioning of the planform in 5° increments. The spool piece had matching upstream and downstream interfaces which allowed the multi-element spool piece to be fit between the existing three-stream rig and the nozzle adapter flanges.

B. Nozzle hardware

The nozzle subsystems, exemplified by the one pictured in Figure 3, were based on the test hardware first used in 2014[6]. As mounted to a variable cycle engine with tip fan, the core stream and bypass fan stream would be internally mixed to produce a warm 'primary' nozzle flow. The tip fan flow would be split in two, with part being directed inside the primary stream, thus inverting the usual velocity profile of a two-stream externally mixed nozzle. The other part of the tip fan flow would be directed to an outer annulus, which in this case is only open for 180° of the azimuth. The nozzle areas were determined by propulsion system studies, discussed in the Introduction, and are given in Table 1. All nozzle subsystems share the same outer nozzle which has the 180° annulus buffer flow nozzle, although in some nozzle designs the portion of the flow directed to this outer annulus was zero, in which case during testing a flow was established in the annulus that matched the flight stream velocity. The symmetry plane of the nozzle mounts on NATR at 22.5° to vertical (in the direction of the overhead microphones) and can be rotated in 45° increments due to the 8-bolt flange pattern.
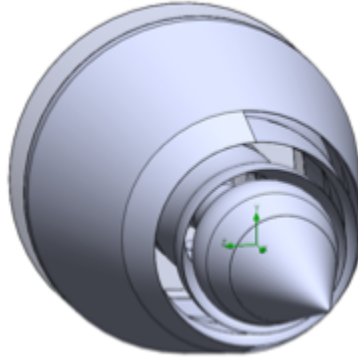
Figure 3 IVP nozzle with outer 180° buffer flow nozzle.

Three main nozzle configurations were tested:

-IV44 was run as a two-stream IVP nozzle with the entire tip fan flow directed to the inner stream and the tertiary stream conditions set to match the flight stream. IV44 was always mounted with the tertiary stream nozzle away from the planform to minimize the possibility that flow nonuniformity from the third-stream duct would cause excess noise on the surface.

-IV19 was run as a three-stream split-tip-flow nozzle. IV19 was mounted either with the center engine planform touching the third-stream opening (IVB19) or away from it (IVS19). With the outboard planform, it was mounted with the planform on the opposite side from the third-stream opening.

-IV01 featured a plug that filled the inner nozzle, removing the inner stream. It was used to represent a single-stream mixed flow turbo-fan (MFTF) nozzle with the third stream matched to ambient flight speed. IV01 was also used as a pseudo-conventional velocity profile nozzle with the tip flow directed completely to the outside (third) stream. The nozzle was 'pseudo-conventional' because the outer fan stream only covered 180° of the azimuth of the nozzle.

Table 1 Nozzle ID, and stream areas.

| Nozzle ID	Area, primary stream, Ac [in²]	Area, inner stream, Ab [in²]	Area, tertiary stream, At [in²]	Ab/Ac
IV44	12.33	5.41	0.00	0.44
IV19	17.35	3.22	4.18	0.19
IV01	17.35	0.2	4.18	0

C. Planform hardware

Three center-engine planform configurations and one outboard-engine planform configuration were tested, as depicted in Figure 4. The center engine planforms were the same except for streamwise length, as given in Table 2. Figure 5 gives a three-view of the medium length center engine planform assembly, with dimensions. The two halves of the aft deck have a 15° dihedral, and the width of the aft deck was 32.6". Note the slight scalloping of the aft deck on the leading edge as the deck meets the pylon. This cutout from the otherwise-constant cross-section airfoil of the deck was put in place to allow the flight stream to flow around the nozzle more like the installed configuration. Figure 6 gives a three-view of the outboard engine planform. The aft deck was at right angles to the pylon/sponson (the pylon of the LM1044 aircraft was roughly square with the aft deck) and the tailfin is at an angle of 150° to the deck and pylon. From the truncated tip of the tailfin to the truncated edge of the deck was 32".

Two nominal dimensions were used in describing the configurations, being somewhat consistent with previous work on jet-surface interaction configurations: planform length and standoff. The planform length, x_E, is defined as the axial distance from the nozzle lip to the trailing edge of the surface. The standoff, h_E, is defined as the radial distance from the geometric lip line to the trailing edge. For the center engine, the pylon blended in to the aft deck at the trailing edge and there were no complications in defining these dimensions. For the outboard engine, the aft deck and tailfin did not end at the same location; the tailfin and aft deck ended short of the trailing edge of the pylon/sponson by 2.4 inches, and were further away from the jet flow by almost an inch. See Figure 7 for further details of these dimensions.

a) central engine   b) outboard engine
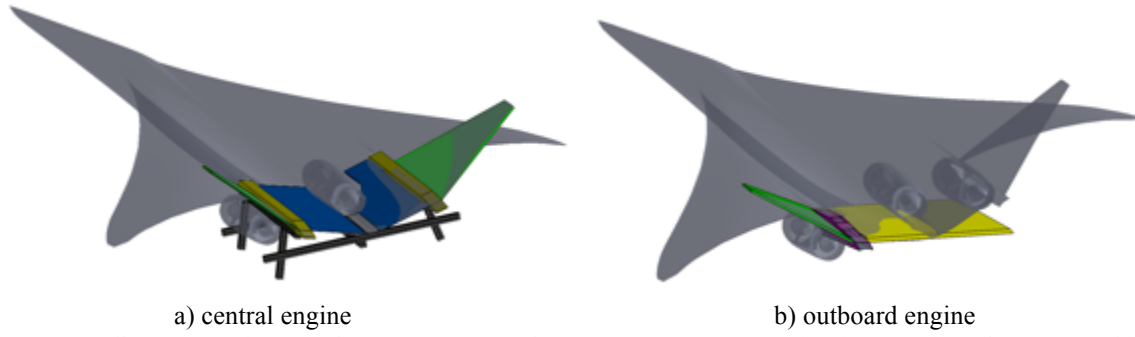
Figure 4 Conceptual image of how model planforms represent the engine installations for the LM1044 conceptual aircraft.
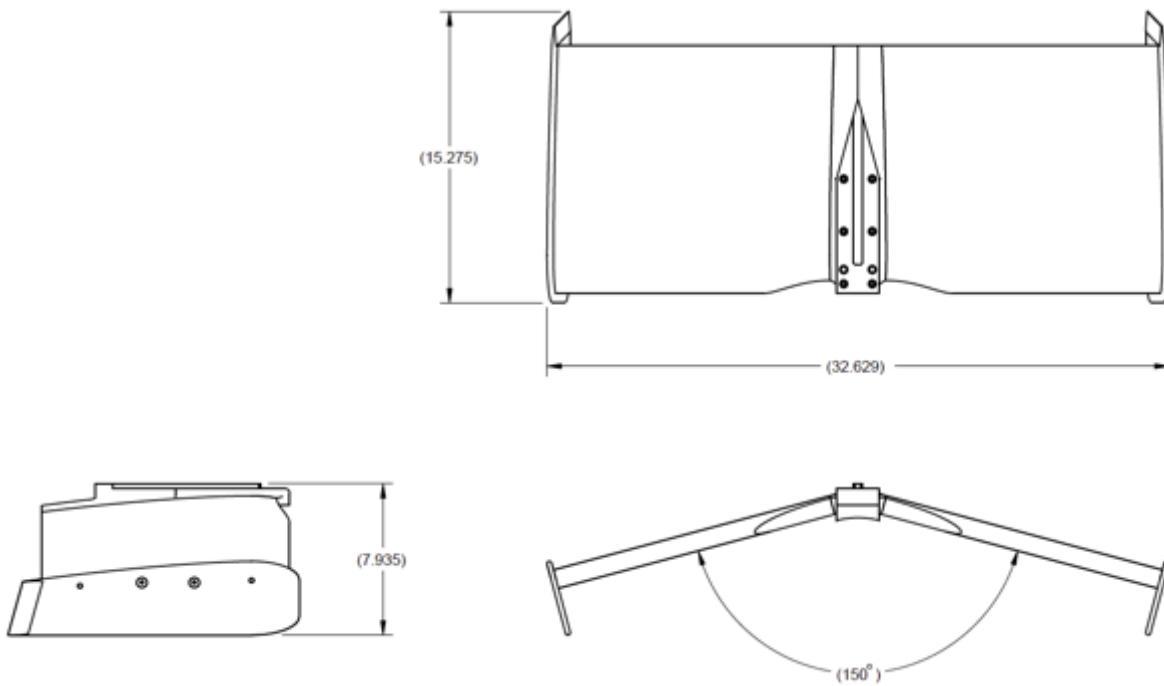
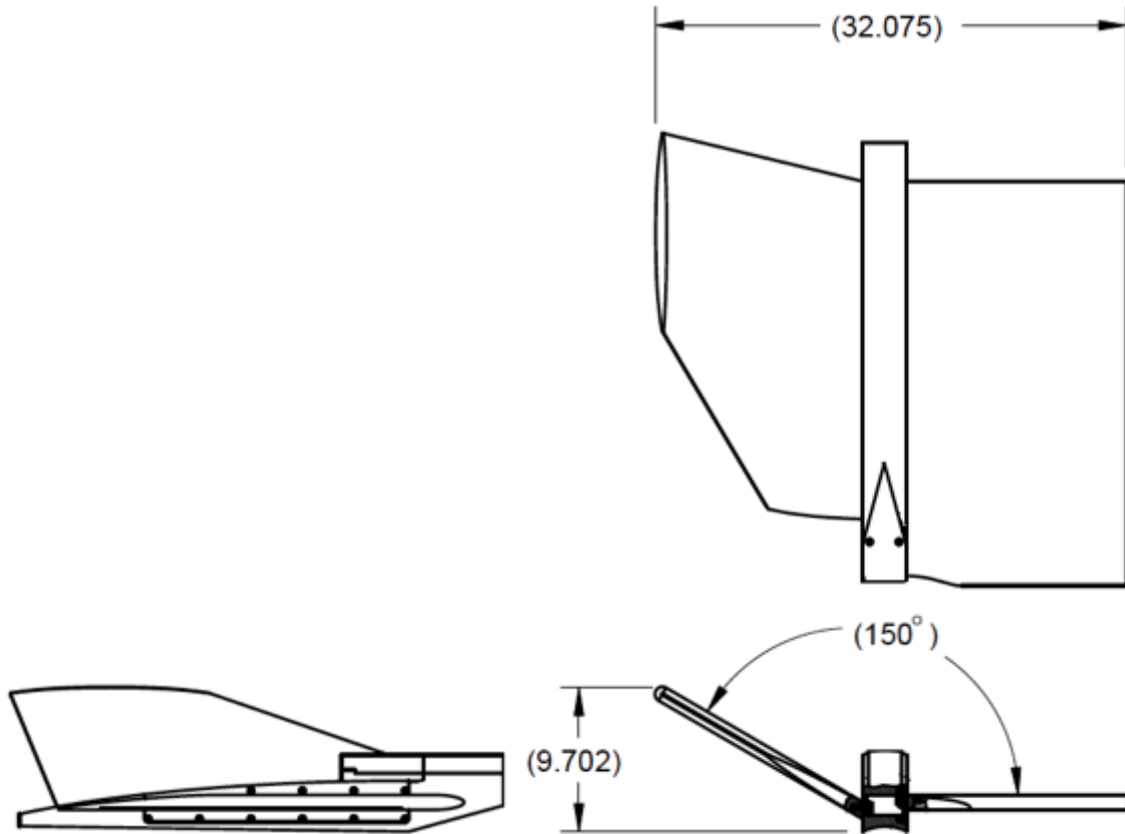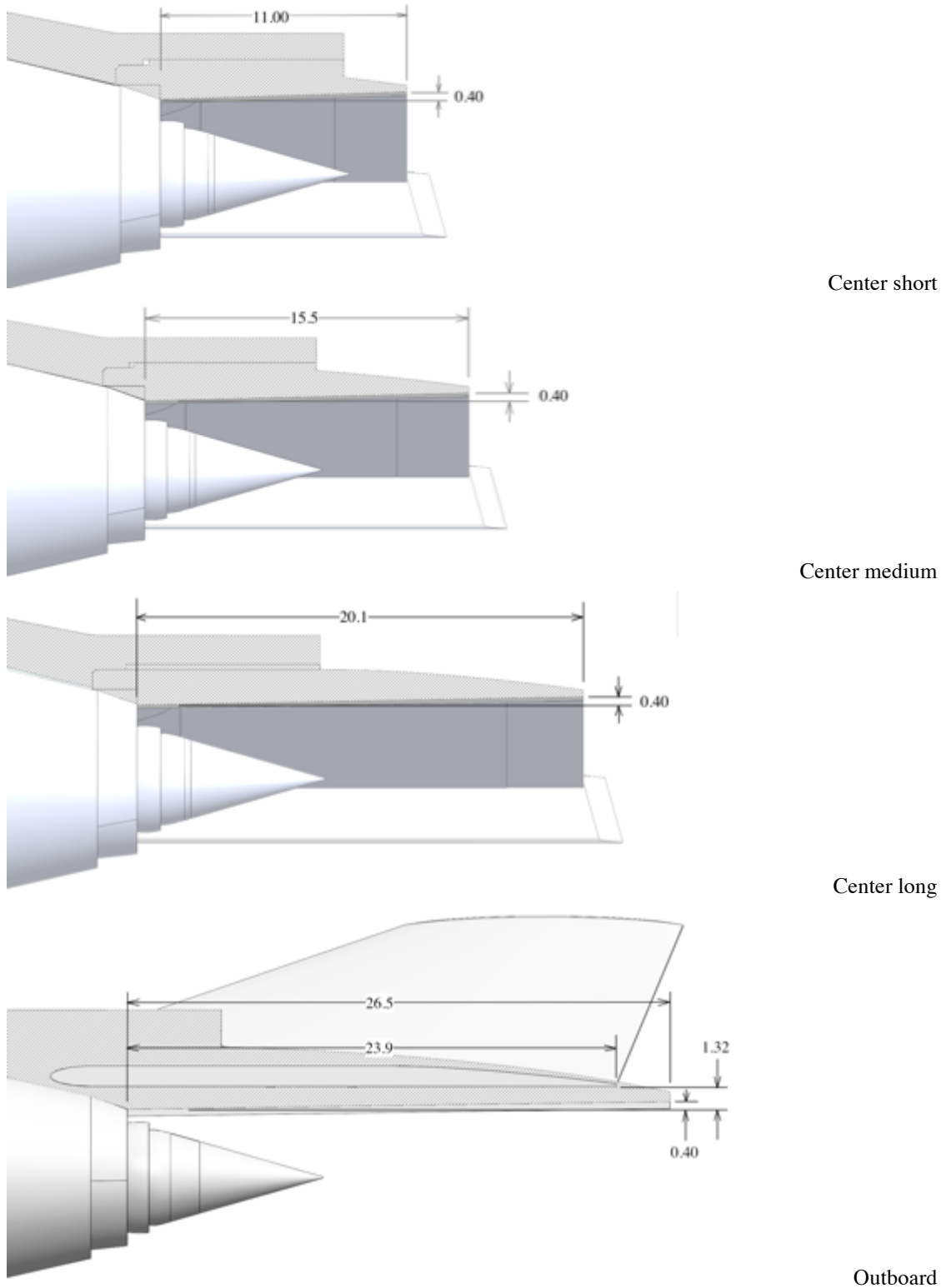**Figure 5 Center engine planform, medium length. Linear dimensions in inches.**

Figure 6 Outboard engine planform. Linear dimensions in inches.

Table 2 Planform configurations, lengths and standoffs.

| Planform ID	Nominal length beyond nozzle, x_E [inch]	Nominal standoff from nozzle lipline, h_E [inch]
Bare	0	0.4
Short	11.0	0.4
Med	15.5	0.4
Long	20.0	0.4
Outboard (pylon)	26.5	0.4
Outboard (deck)	23.9	1.32

Center short

Center medium

Center long

Outboard

Figure 7 Planforms: Lengths and standoffs for installed planforms. Linear dimensions in inches.

D. Hardware configurations

Various combinations of the three nozzles, decks and support arm subsystems, operated over sets of flow conditions (setpoints) simulated the different engine designs for all the installation locations and observer angles. Figure 8 shows one hardware configuration.
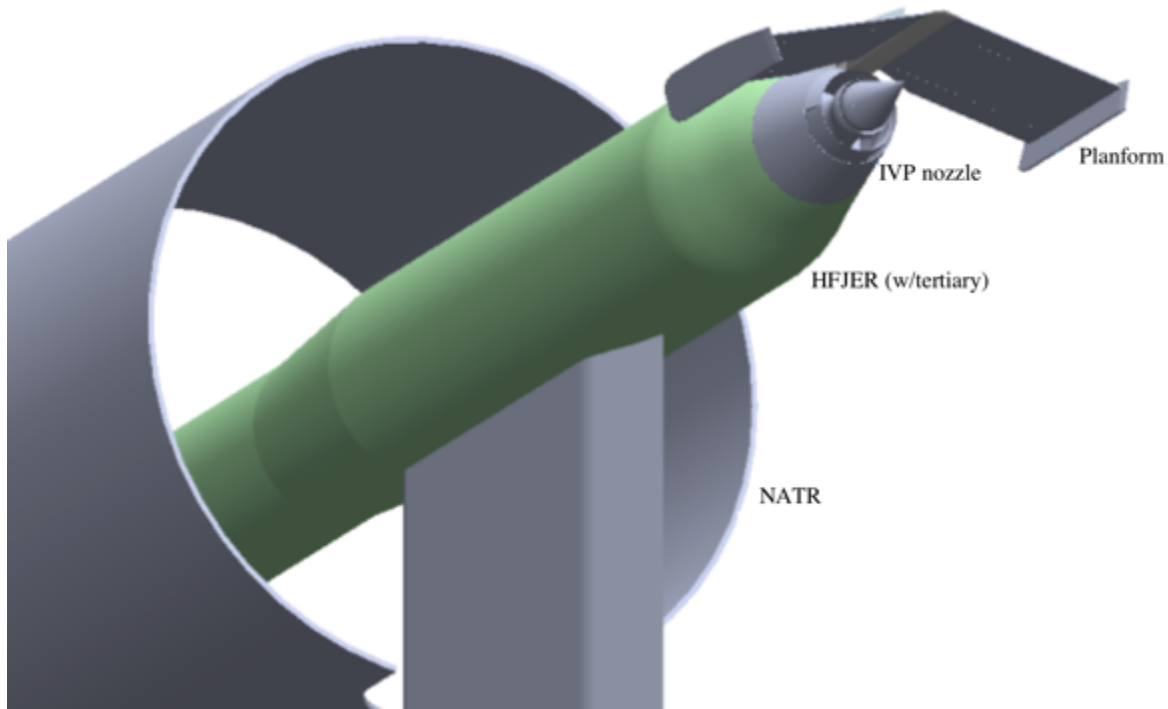

Figure 8 Hardware configuration overview, NATR, jet rig, nozzle system, and planform.

Configurations were specified in combinations of nozzle system, nozzle orientation, planform, and planform orientation. The nozzle systems are identified in Table 1, and the planforms in Table 2. The orientations of the nozzle and planform are given by the angle of the symmetry plane (the 180° buffer stream gives the nozzle system bilateral symmetry) to the acoustic observer. Because configurations could easily be confused, cartoon graphics were prepared with the daily run sheets for most of the test to assure that the hardware matched the desired configuration. The cartoons included the nozzle ID with orientation (in the technicians' terms), the planform ID with angle from the graded scale on the rig, and the research configuration name. See Figure 9 for an example of the visual representation of the naming convention.

The far-field microphones ('observer') were located roughly 30° off the vertical in the facility (counterclockwise looking upstream). For the phased array, the 'observer' was located 45° from the vertical.

The buffer stream nozzle had 45° increments in its rotation, which sets a hard limit on the azimuthal angles tested. When the nozzle orientation code says '0°', the nozzle symmetry plane was physically at 22.5°, roughly aligning with the overhead microphones. When the orientation code says 'S60' to simulate a noise certification test's lateral observer at 60° azimuthal angle up from the nadir, the nozzle system was rotated 45°, with the symmetry plane at an actual angle of 72.5° to vertical.

The planform could be rotated and locked into position every 5°. The planform angle was set to be exactly at the specified angle relative to the microphones for both far-field and phased microphones as each system was tested.

a) center engine installation   b) outboard engine installation
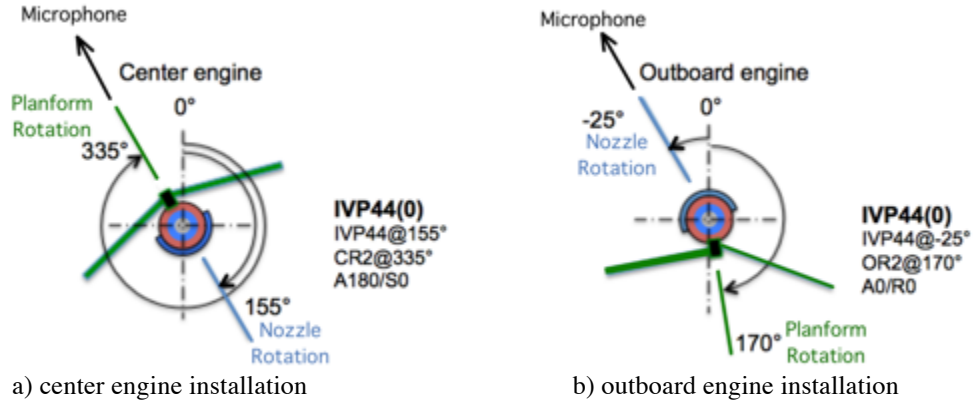
Figure 9 Naming conventions for configurations, nozzle and deck clocking.

    The configurations of nozzle and certification observer (represented by the overhead microphone plane) that were possible are given in Figure 10 (center engine) and Figure 11 (outboard engine). Not pictured here, all the center engine configurations have three lengths of planform, as given in Figure 7. This was specified by *Short, Med, or Long* designation. The outboard engine configurations had only one planform length, called out as *Outboard* in Table 2. The uninstalled, isolated nozzle configuration was labeled *Bare*. In these figures, the IV44 nozzle is identified as IVP44 with its rotation noted in parentheses. The IV19 is identified as either IVPS or IVPB depending upon whether the tertiary annulus was away from, or next to, the planform.
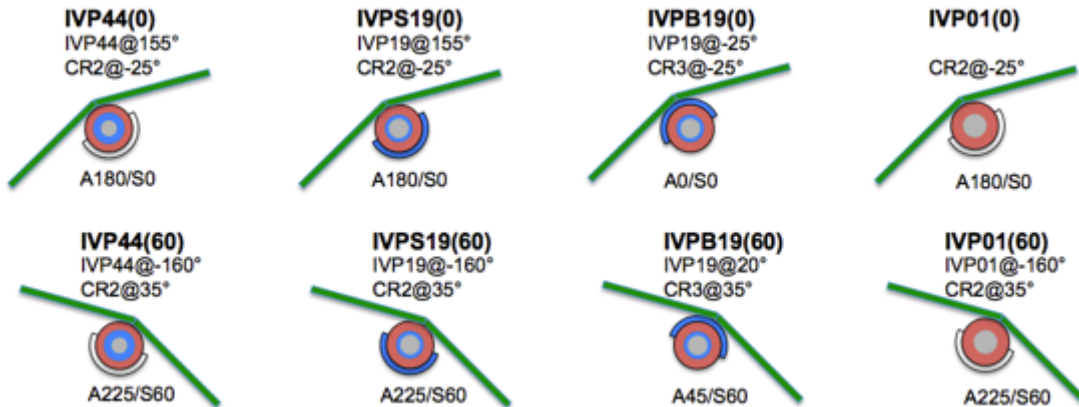
Figure 10 Possible test configurations for center engine. Not illustrated: each configuration can have three lengths of deck applied. In the cartoons, red signifies the hot primary flow and blue the cold tip flow. Cases without tertiary stream (IV44 and IV01) have white color.
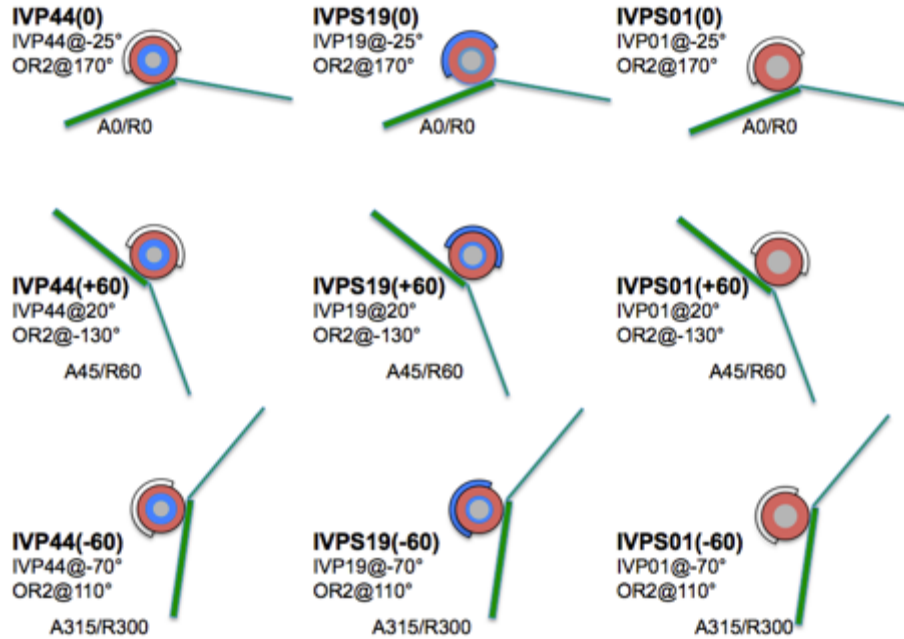
Figure 11 Possible test configurations for outboard engine. Only one planform was available and the nozzle clocking relative to the planform was the same for all configurations. The thin planform line represents the tailfin, thick line represents the deck.

V. Flow conditions and setpoint definitions

The flow conditions for this test originate in system-level engine designs created independently by NASA for the *LM1044* concept aircraft, pictured in Figure 1. There were eight engine designs chosen, plus one research test flow for the rig. The engine designs were arbitrarily identified by a serial number ('EngineID') from this study. The values of the key design variables for the engines are given in Table 3. Each engine design was matched with a nozzle having appropriate exit areas. All engine designs had a sea-level-rated T4 of 3400R and an overall pressure ratio of 43. For each engine, five throttle points, running from 60%-100% throttle, were acquired from the engine performance maps as they would operate at 1000' altitude and $M_{flight} = 0.35$ flight speed. These throttle lines became the basis for the flow setpoint matrices used in the test.

One additional 'engine' flow matrix was run for a limited number of configurations: EngineID 770. This flow matrix ran the inner two streams at unheated speeds corresponding to setpoints in the Tanna[7] matrix. These points were used to repeat databases from previous jet-surface interaction tests[8,9] taken at the same flow conditions using a single-stream nozzle. One of the objectives of the current test is to add the effect of the flight stream to these models of jet-surface interaction.

Although the facility is capable of producing $M_{flight} = 0.35$, most flow setpoints were acquired at flight speed $M_{flight} = 0.3$. Because the design flight speed at takeoff was actually $M_{flight} = 0.38$, the sensitivity to flight speed was assessed at the designated takeoff point by acquiring three flight speeds: $M_{flight} = 0.25, 0.30, 0.35$. This allowed extrapolation of the propulsion exhaust noise to the design flight speed.

Definitions of the setpoints for lateral certification point in each engine cycle are given in Table 4. The conditions are given in terms of the three-stream HFJER rig streams (core 'c', bypass 'b', tertiary 't'), but note that the rig core stream is actually feeding the nozzle primary stream, and the 'bypass' stream is actually feeding the inner-most nozzle annulus. Also, note that because the bypass and tertiary streams of the rig have a common temperature control, there is no independent specification for temperature on the outer fan stream, NTRt. In setpoints where the tertiary stream has an NPRt less than 1.1 (such as for the IV44 nozzle system) the tertiary stream was operated such that the its velocity matched the flight speed, producing a true inverted velocity nozzle, not a split-tip-flow system.

Table 3 Engine cycle and nozzle combinations.

Lateral throttle	EngineID	tipBPR	Design FPR	NozzleID	Linear scale factor
100%	1549	0.49	1.8	IV19	11.84
100%	1648	0.49	1.8	IV44	14.00
100%	2044	0.005	1.8	IV01	14.00
100%	1747	0.29	1.8	IV01	13.28
90%	2056	0.005	1.9	IV01	13.09
80%	1573	0.49	2	IV19	12.18
80%	1672	0.49	2	IV44	12.82
80%	2068	0.005	2	IV01	12.38
N/A	770			IV19	

Table 4 Engine cycle (takeoff) setpoint definitions.

EngineID	Throttle, %	Setpoint	NPRc	NPRb	NPRt	NTRc	NTRb	Mf
1549	100	156	1.775	1.844	1.844	1.704	1.239	0.35
1648	100	256	1.775	1.844	1.091	1.704	1.239	0.35
2044	100	356	1.7778	1.000	1.091	1.538	1.000	0.35
2056	90	449	1.8049	1.000	1.091	1.554	1.000	0.35
1573	80	536	1.723	1.898	1.898	1.712	1.242	0.35
1672	80	636	1.723	1.898	1.091	1.712	1.242	0.35
2068	80	736	1.808	1.000	1.091	1.574	1.000	0.35
1747	100	855	1.7762	1.000	1.8779	1.641	1.245	0.35
770	N/A	1550	1.429	1.429	1.000	1	1	0.00
	N/A	1551	1.429	1.429	1.007	1	1	0.10
	N/A	1552	1.429	1.429	1.016	1	1	0.15
	N/A	1553	1.429	1.429	1.028	1	1	0.20
	N/A	1554	1.429	1.429	1.045	1	1	0.25
	N/A	1555	1.429	1.429	1.064	1	1	0.30
	N/A	1556	1.429	1.429	1.091	1	1	0.35
	N/A	1770	1.856	1.856	1.000	1	1	0.00
	N/A	1771	1.856	1.856	1.007	1	1	0.10
	N/A	1772	1.856	1.856	1.016	1	1	0.15
	N/A	1773	1.856	1.856	1.028	1	1	0.20
	N/A	1774	1.856	1.856	1.045	1	1	0.25
	N/A	1775	1.856	1.856	1.064	1	1	0.30
	N/A	1776	1.856	1.856	1.091	1	1	0.35

VI.   Instrumentation

A. Far-field acoustics

An overhead 24-microphone arc array was used to measure far-field spectral directivity using ¼" microphones, Model 4939 from Bruel & Kjaer. Matching ¼" Bruel & Kjaer preamps were used along with Bruel & Kjaer Nexus power supply/signal conditioner. Data were acquired on a digital recorder with a 190kHz bandwidth, and transferred to a Linux computer for processing. End-to-end *in situ* calibrations of the microphones using a Bruel & Kjaer 124dB pistonphone was performed weekly, with no deviations being recorded greater than the uncertainty of the pistonphone over the course of the test.

Acoustic data were processed to account for individual microphone sensitivity and spectral characteristics, refractions due to propagation through the freejet flight stream, and losses due to atmospheric attenuation. The resulting spectral directivity, at model scale with atmospheric attenuation restored, was the starting point for analysis and synthesis of flyover noise.

B. Acoustic Phased Array

An acoustic phased array was used to identify noise source distributions and to confirm that the truncated planform adequately simulated the acoustically important aspects of the Lockheed Martin 1044 aircraft for propulsion noise. The array had 48 condenser microphones with a 5-30kHz range. The microphones were arranged in a 5-spiral-arm pattern with a 39" diameter. The array was deployed at a polar angle of 90° to the nozzle plug tip, at an azimuthal angle of 45° to the vertical, and a distance of 6.5 feet from the jet centerline; see Figure 1. The positioning of the array was chosen to allow a similar view angle as the overhead array while keeping the support structure out of the flight stream. Note that the model was rotated to be in the same azimuthal orientation relative to the phased array and to the far-field microphones.

C. Particle Image Velocimetry (PIV)

Mean and turbulence velocity measurements were made using particle image velocimetry (PIV) in a manner consistent with recent tests in NATR[10,11]. Two types of PIV measurements were performed: (1) two-component streamwise experiments and (2) cross-stream three-component PIV experiments. Figure 12 shows a representation of the PIV equipment in both streamwise and cross-stream optical orientations. For all PIV studies, cameras with 2.6K x 4K CCD arrays were used to record images. For the streamwise experiments, four cameras, each with a 380 by 325 mm field of view, were used in a two-by-two configuration with a 28 mm overlap between camera images. This produced an instantaneous field of view of 367 by 585 mm. This field of view was traversed downstream, with overlap, for 6 locations yielding an aggregate data set 1891 by 585 mm. The laser and beam forming optics were carried on a large axial traverse with 0.1mm positional accuracy. The light sheet source was a 400 mJ per pulse, 532 nm, dual-head Nd-YAG laser with the vertical laser sheet fanning from optics below the jet centerline. The light sheet was positioned approximately 2mm behind the jet centerline from the cameras to remove the flare from the round nozzle parts from reaching the cameras.

In the cross-stream experiments, the laser light sheet was identical to the streamwise configuration aside from the 90° rotation of the cylindrical lens. A stereo pair of 2.6K x 4K CCD cameras, were mounted downstream approximately ±37° off the jet centerline in the horizontal plane. When combined, the field-of-view for the reconstructed three-component velocity field was 393 by 322 mm. Ten axial stations were acquired for all model configurations.

For all PIV experiments, all of the HFJER streams were seeded with a pH stabilized dispersion of aluminum oxide (0.4 µm particles) in ethanol. The free jet was seeded with a combination of oil-based foggers. A 'spray-bar' manifold across the opening of the air intake of the freejet was fed with a pair of foggers, while two foggers positioned in the air inlet house supplemented the high flow conditions. All foggers were using oil-based fog fluid and generated 0.5 to 4.5 µm particles.

Two-dimensional vector maps from the individual cameras were generated using a multi-pass processing approach. The processing strategy used an initial pass with 64 by 64 pixel subregions on 32 pixel centers followed by 6 passes (using simulated annealing) at 32 by 32 pixel subregions on 16 pixel centers, followed by two final passes using subregion distortion processing. Symmetric Phase Only Filtering was used on the cross-stream data sets to reduce the effect of flare light from the model. All PIV surveys used 400 image pairs per axial station, yielding 400 velocity vector maps at each axial station. The velocity vector maps were then ensemble averaged to compute the first and second order statistics. Hard velocity cutoff limits and Chauvenet's criteria were used to remove outliers before computing statistics.

In planning for the test, it was assumed that a light sheet dump would be needed on the planform to keep the lightsheet from scattering from the surface into the PIV cameras, when cross-stream PIV was being acquired[12]. In anticipation of significant flare light being scattered from the planform surfaces, replacement panels were made with grooves cut into the surface to capture the laser light and prevent the camera from seeing the resulting flare light from the surface. During testing, the panels would have to be replaced for each axial station of the laser light sheet since grooves could not be tolerated upstream of the measurement plane. This would have been very slow in testing; luckily this was found to be unnecessary. While the light sheet did cause data to be lost very near the surface, it did not cause damage to the cameras and hence was considered acceptable. In the interest of test time, the grooved panels were not used.
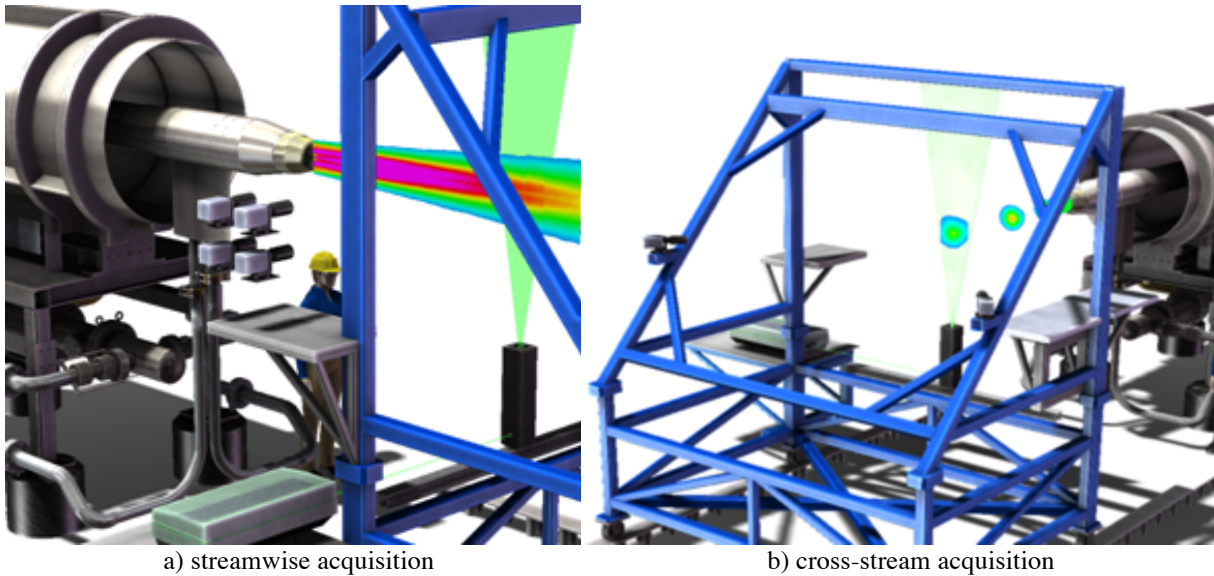
| a) streamwise acquisition | b) cross-stream acquisition |

Figure 12 PIV setups with measurement planes illustrated.

VII.   Key Findings from Objectives

Far-field spectra for roughly 850 configuration/conditions were acquired during the test. Data will be shown here as it supports the test objectives. Spectral directivity data presented here were processed to a 1 foot, lossless condition in model-scale using the NASA Digital Acoustics Data System (DADS) software. Where necessary, the highest frequencies were trimmed to remove the digital noise floor.

EPNL values were obtained by scaling the data to full-scale, Doppler-shifting the data for flight, integrating it to a 1/3 octave spectral directivity, and writing out the 1/3 octave spectra in a tabular format. The data was read into the NASA Aircraft Noise Prediction Program (ANOPP) as a source, where it was numerically flown, in keeping with FAR36 rules, at a constant speed and a constant altitude of 1000 feet, including ground effects, past the lateral observer 4 feet above ground at a 1467-foot sideline. The sources were imported into ANOPP as three engine spectral directivities, each engine directivity having been acquired at the appropriate azimuthal angle while installed on the planform. These sources, therefore, include the effects of installation and forward flight directly.

### A. Validate representation of LM1044 by test hardware (Objective 1)

Beyond performing checks on the data for errors caused by rig noise, background levels, or improperly functioning instrumentation, it was important to validate that the model-scale hardware represented the aspects of the full-scale aircraft pertinent to aft propulsion noise. Two issues were identified in the design of the model-scale hardware: *adequacy of planform representation for acoustics*, and *similitude of ambient flow around the nacelle/nozzle*.

Confirm that test model planform has adequate coverage to reproduce the shielding of the aircraft (Objective 1a)

A key assumption in the development of the planforms used to model the aircraft in this installed propulsion test was that surfaces away from the jet plume could be truncated without loss of fidelity in either the flow around the nozzle and plume, or in the acoustic shielding provided by the aircraft body. To assess whether sound was radiating 'through' the missing parts of the aircraft, source distributions around the truncated edges were measured using the phased array. The planform was angled toward the phased array in the same orientation as they would be to the far-field microphones, and data were acquired at polar angle 90°. The case with the most shielding was the 'center engine' configuration, at a flyover observer location.

As demonstrated for two frequencies in Figure 13 and Figure 14, the source distribution maps showed no significant sources around the upstream and side edges where the truncated airframe would have been. However, the phased array data, processed using robust functional beamforming, have only a 10dB dynamic range, so sound less than 10dB below the peak leaking around the edge would not be seen in these plots. To quantify the error in the radiated sound passing around the edges of the planform, the source maps were integrated over different regions of interest and compared. First, the entire map was integrated, this being the total sound that the far-field microphones

would have measured. Then, the sound coming from upstream of the trailing edge was integrated, this being the erroneous sound leaking from edges where an airplane should have blocked it. Finally, the sound coming from downstream of the trailing edge was integrated, this being the sound reaching the far-field microphones if the entire airplane body had been in place. As seen in the spectra of Figure 13, the sound coming from the truncated edges was very small for most frequencies of interest, 10-15dB below the noise produced downstream of the trailing edge. The difference between the total and the downstream region was less than 0.2dB. This represents the error produced by truncating the planform. At low frequencies (Figure 14), where the spectra show the upstream sound to be near to the total in sound amplitude, the source maps show that most of the upstream sound is actually the tails of the point spread function of the beamforming, rather than noise coming from upstream of the truncated edges. This confirms the validity of using the truncated planforms.
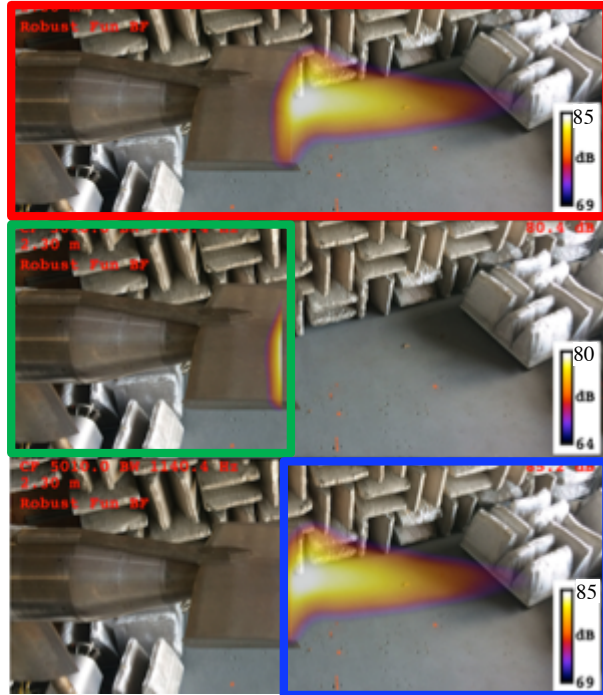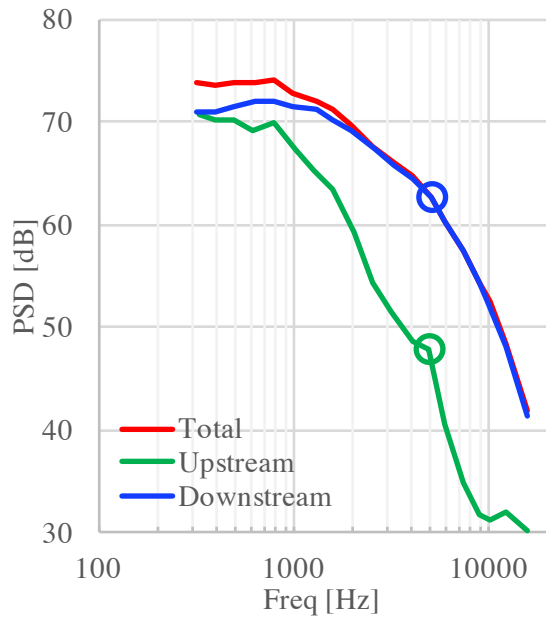
Figure 13 Source distributions and sound spectra from integrating source maps at 5000Hz. Total (red line), upstream (green line) and downstream (blue line) of trailing edge.
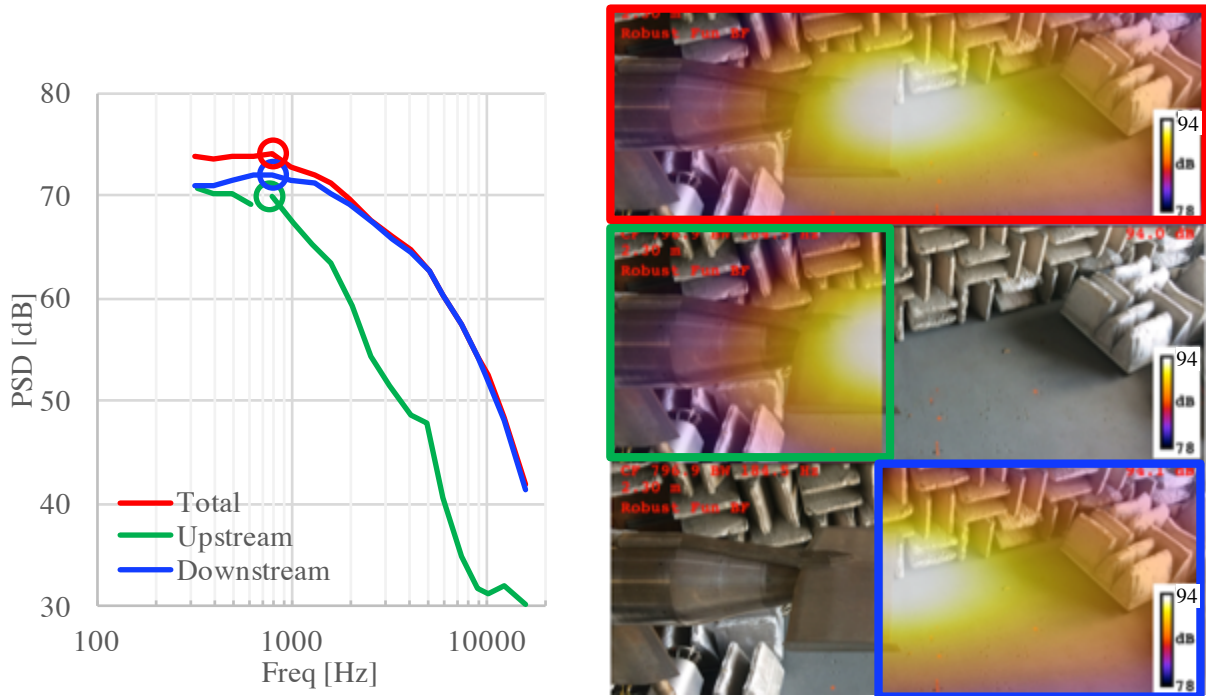
Figure 14 Source distributions and sound spectra from integrating source maps at 800Hz. Total (red line), upstream (green line) and downstream (blue line) of trailing edge.

Aero simulation of nozzle-planform region (Objective 1b)

One of the key problems in designing the test hardware was how to accommodate the large diameter of the jet rig relative to the aircraft's engine nacelle. The leading edge of the planform was cut back as far downstream as possible to avoid building up a separation region at the junction of the planform and the rig. Additionally, the leading edge was scalloped at the rig to scoop as much freejet flow as possible into the region where the pylon and nozzle meet. The initial PIV runs were focused on looking at this region, at a plane just downstream of the primary nozzle (second annulus). Optical access was extremely challenging and the results require some interpretation since only one of the stereo cameras could see the region. The result is shown in Figure 15 in two views. The overall impression is that the nozzle is surrounded by a thick boundary layer from the rig, which is to be expected given the large size of the rig. The region of zero velocity just downstream of the inner nozzle is misleading; that stream was flowing but was not seeded. Below the nozzle, there is a trace of the wake from the strut that feeds the rig. The right camera is blocked by the plug but can just barely see a portion of the flow between the nozzle and the planform on the upper left. Here the flow is 65 m/s, which is about the same velocity as other locations with the same radius from the rig. There is some asymmetry to the flow, the right side being 5-10 m/s higher than the left, and on the right side near the planform surface the rig has a reduced boundary layer.

In spite of these imperfections, the design did avoid having stagnation zones near the nozzle. There may be some increase in high frequencies due to an increased shear near the nozzle but it should not be inhibiting.
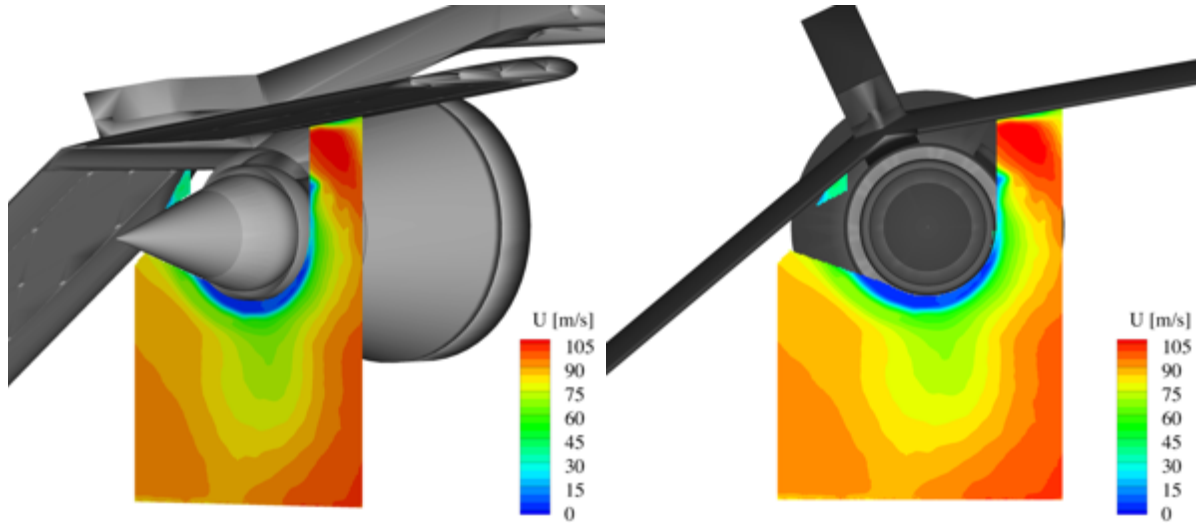
Figure 15 Two views of velocity acquired at primary nozzle exit plane of IV44 nozzle with short center planform for setpoint 255 (M_{flight} = 0.3).

B. Estimates of total aircraft exhaust noise (Objective 2)

Getting an estimate of the total exhaust noise of the aircraft when it has three engines with unique installation impacts requires the noise from each installed engine to be measured and summed before scaling up and transforming to flight. While the two outboard engines are similar, the installation impact for an observer on one side of the aircraft flight path will be different for each. This is why so many planform rotations were acquired, and since the lateral observer was considered the most relevant to estimating total certification noise, this observer angle was given priority when downselecting configurations to be tested.

The next set of figures shows how the 1-foot radius, lossless model-scale data, in power spectral density (PSD) were transformed into the exhaust-component EPNL. Scaling is an important part of this, as is atmospheric attenuation and the human spectral response.

Starting with the model scale data, the top row of Figure 16 shows the three spectral directivities, one for each installed engine, measured at the same throttle point for the lateral observer on one side of the vehicle. For the center engine, this means the measurement made at the S60 planform rotation. For the outboard engines, this means measurements made at R60 and R300 for the two underwing engines. In the figure, the large vertical scale (height in the carpet plots) does not readily bring out the differences in installation, but there are small differences in the color that show that the outboard engines are louder than the center engine. It is also evident upon examination that the two outboard engine locations have different sound levels, showing the importance of azimuthal directivity across the airplane due to the installation. The bottom plot in the figure shows the sum of the acoustic power from the three individual measurements, just as an observer would receive from the total aircraft.

a) Center engine (S60)   b) Right outboard engine (R60)   c) Left outboard engine (R300)
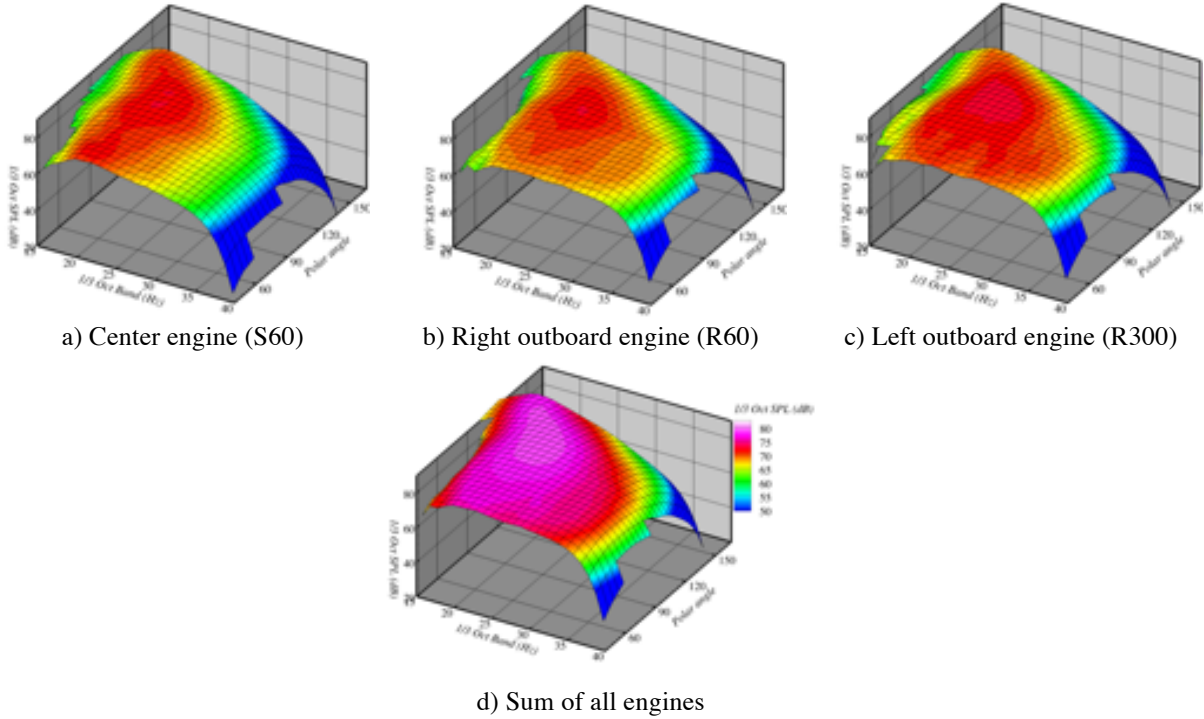

d) Sum of all engines
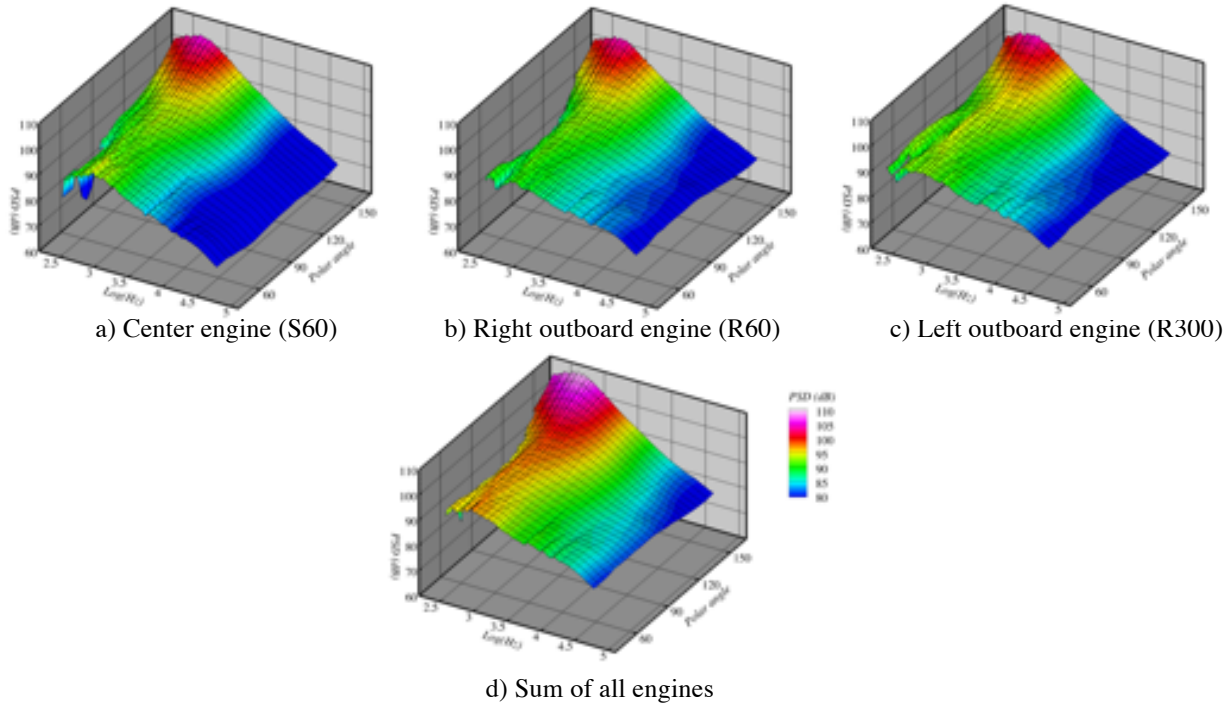
Figure 16 Demonstration of compilation of propulsion sources for simulation of aircraft flyover noise. Spectral directivity of PSD, 1-foot radius, lossless, at model scale for IV01 nozzle operating at setpoint 455, and installed on the Medium planform as observed by lateral observer.
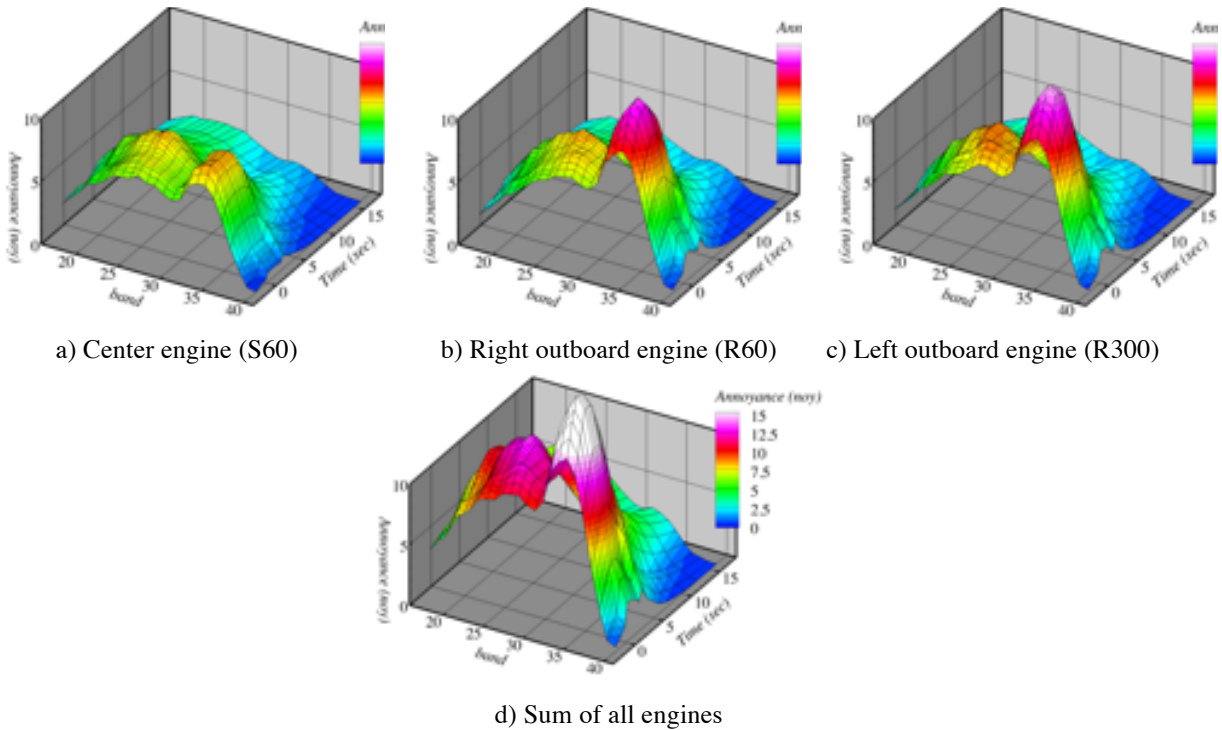
The next figure (Figure 17) shows how the spectral directivities change as they are transformed to full scale, then propagated over the distance to the lateral observer on a standard day with a Doppler shift applied. The biggest change is that the high frequencies are greatly reduced by the atmospheric attenuation. It appears that there is a very broad peak across more polar angles as the increased distance to the observer at aft angles negates the increase in noise directed aft.

The next step in simulating the flyover noise is to weigh the 1/3-octave spectral directivity by the human frequency response, producing maps of annoyance (Figure 18), given in units of noy, and transforming the angular coordinate to a time coordinate with flight speed, flight path, and observer location. From here, the EPNL is essentially the volume integral under the annoyance surface. The plots of annoyance really show what part of the jet spectra matters to the EPNL metric. Note how the human frequency response raises a strong peak at 2.5 kHz near the broadside angles. The fact that annoyance is a linear scale, compared with the logarithmic (dB) scale used in the other spectral directivities, accentuates the peak. Also, note that the annoyance is a nonlinear metric and the total annoyance is not the sum of the three annoyance plots but is computed strictly from their combined PSD. They are shown here individually for insight.

Strictly speaking, the method for computing EPNL from the annoyance involves a bit more than a simple integral, first integrating over frequency to produce PNLdB as a function of time, and then integrating over time, truncating the integration at the 10dB down points coming and going. There are corrections for tones, which usually factor in mixing noise only if ground reflections were included in the propagation to the observer. These corrections were not included in the figures shown here, but were applied in the final EPNL calculations.

a) Center engine (S60) b) Right outboard engine (R60) c) Left outboard engine (R300)


d) Sum of all engines

Figure 17 Demonstration of compilation of propulsion sources for simulation of aircraft flyover noise. Spectral directivity of 1/3 octave SPL, lateral observer position, standard day, full scale for IV01 nozzle installed on Medium planform.

a) Center engine (S60) b) Right outboard engine (R60) c) Left outboard engine (R300)

d) Sum of all engines

Figure 18 Demonstration of compilation of propulsion sources for simulation of aircraft flyover noise. Spectral directivity of annoyance, lateral observer position, standard day, full scale for IV01 nozzle installed on Medium planform.

When the methodology was applied to all engine/nozzle combinations for the base *LM1044* aircraft (e.g., medium planform on the center engine), using ANOPP to transform to flight conditions and calculate EPNL, the resulting

lateral EPNL (using all three engines) versus throttle line for the seven selected engine/nozzle combinations are as given in Figure 19. Recalling that the surrogate metric for Tech Challenge success was 93.3EPNdB, all the engines with nozzle pressure ratio (NPR) of 1.8 at 100% throttle (solid markers in plot) were below this level at 100% throttle. The engineID 2056, which was a mixed-flow turbofan with NPR=1.9, also met the goal at 100% throttle. The MFTF (nozzle IV01) and the basic IVP nozzle (IV44), when mounted on engines with NPR=2.0 at 100% throttle, met the goal if their throttle was reduced by roughly 10%, using a programmed lapse rate during takeoff, or to a flow condition with NPR≈1.83. Only the IVP nozzle with 50% of its mass diverted to the outer buffer stream (IV19), failed to meet the goal when the throttle was reduced to NPR=1.83.
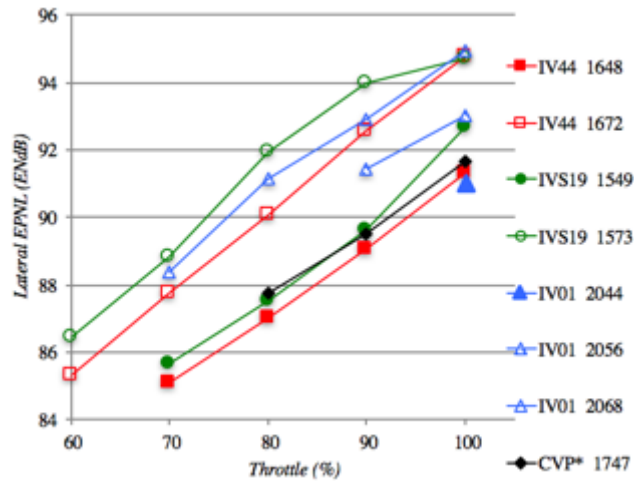
Figure 19 Final lateral EPNL for the installed exhaust noise for the LM1044 with various engine/nozzle combinations.

C. Add flight effects to Jet-Surface Interaction database (Objective 3)

1. *Effect of flight on noise in Jet-Surface Interaction modeling*

Considerable work has gone into building a database describing how jet noise is impacted by the presence of a surface parallel to the jet centerline. Impacts of variables such as surface length, standoff, and spanwise width have been thoroughly documented for a single-stream jet at various speeds[8,9,12]. Variations in jet temperature, and even multiple-stream nozzles[4], have been explored. One major variable as yet untouched is the flight stream speed; all data to date were acquired with a static nozzle. Given the extreme impact of flight speed on jet noise, and the differences in source type, mixing noise quadrupole versus trailing edge dipole, the impact of flight should be significant.

To measure how the installed jet noise changes with flight speed for a simple, single-stream jet, the IV19 nozzle was run over a range of acoustic Mach numbers (cycle 770, matching Tanna's matrix[7]) for a range of flight speeds ($M_{flight} = 0.0 - 0.35$). One approach for analysis would be to separate the trailing dipole from the mixing noise using spatial coherence, as has been in the past. A detailed analysis of this is being presented at this same conference[13], and will not be discussed here.

2. *Effect of flight on source distribution of uninstalled jet mixing noise*

The equivalent single-stream, unheated jet case was also used to measure the impact of the flight stream on jet noise source distributions as measured by a phased array at 90° to the jet. Earlier tests[14] showed that a flight stream elongates a jet plume. This led to the expectation that the flight stream would elongate the source distribution as well. Surprisingly, this was not what was found.

In Figure 20, a plot shows how the noise spectra measured by the phased array reduces in amplitude as flight speed increases. Also in the figure are a series of source maps, one for each flight speed, for the 2,500Hz frequency band (roughly $St_D=1$). The source strength colorscale of each map is adjusted, with a dynamic range of 10dB from its peak. The source maps were created using conventional beamforming, accounting for the convection of the sound across the flight stream. The strength of the downstream sources is reduced, in keeping with the lower shear with

flight, and the sources near the nozzle become stronger relative to the main source field. However, the source distribution is found not to lengthen downstream with increased flight speed as had been expected.

The fact that the source distribution did not stretch with flight speed is in conflict with the observations of the jet plume. The plume, as measured by PIV, does stretch with flight speed. Mean and turbulent velocities, acquired with PIV for this nozzle at three of these flight speeds, are shown in Figure 21. As shown by the superimposed lines in the figure, the potential core does lengthen with flight speed. As expected from the decrease in source strength, the turbulent velocities (right-hand column of Figure 21) also decrease in strength with flight speed. The decrease in turbulence levels is proportional everywhere, including the region alongside the plug of the nozzle where the source density does not change as rapidly with flight. This is shown more convincingly by the line plots of the turbulent energy along a line through the shear layer (at a constant radius), given in Figure 22. The location of this line is shown by the dashed line in Figure 21. For reference, the axial origin is the primary nozzle exit, and the plug tip is at x = 8.4". The relative reduction in turbulent velocity is the same over all axial regions found by the phased array to have acoustics sources (Figure 20). From this, we speculate that the difference in scaling in this region is due to the proximity of the sources to the solid surface changing the acoustic nature of the sources, and not due to the boundary layer of the rig maintaining a strong shear in the initial portions of the shear layer near the nozzle.
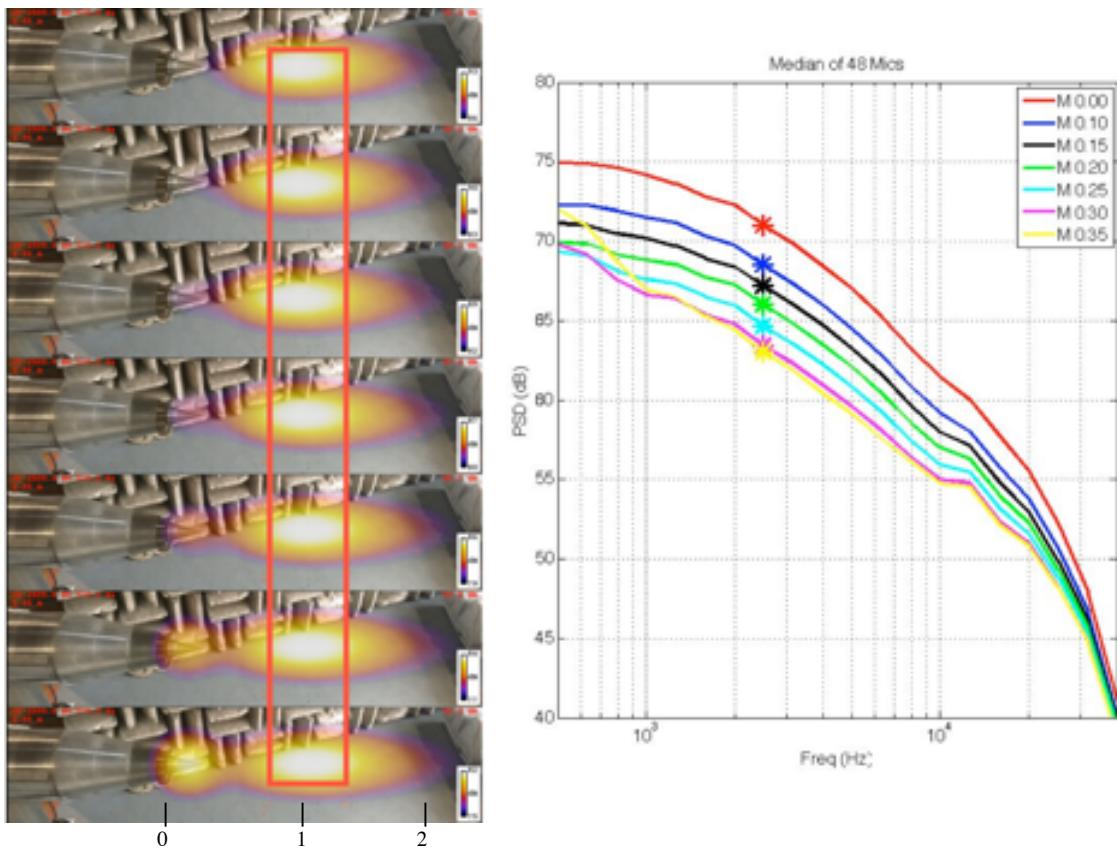
Figure 20 Source maps for single-stream, Ma = 0.9 jet, operating in different flight streams, M_{flight}=0—0.35 in 0.05 increments. The frequency of the maps is 2500Hz. The maps have a red box superimposed to gauge how source distribution does not change with M_{flight}. On the right, spectra measured by the phased array, showing how the jet noise amplitude is reduced with increasing flight speed.

M_{flight}=0.0

M_{flight} =0.2

M_{flight} =0.3

a) Mean axial velocity   b) Variance of axial velocity
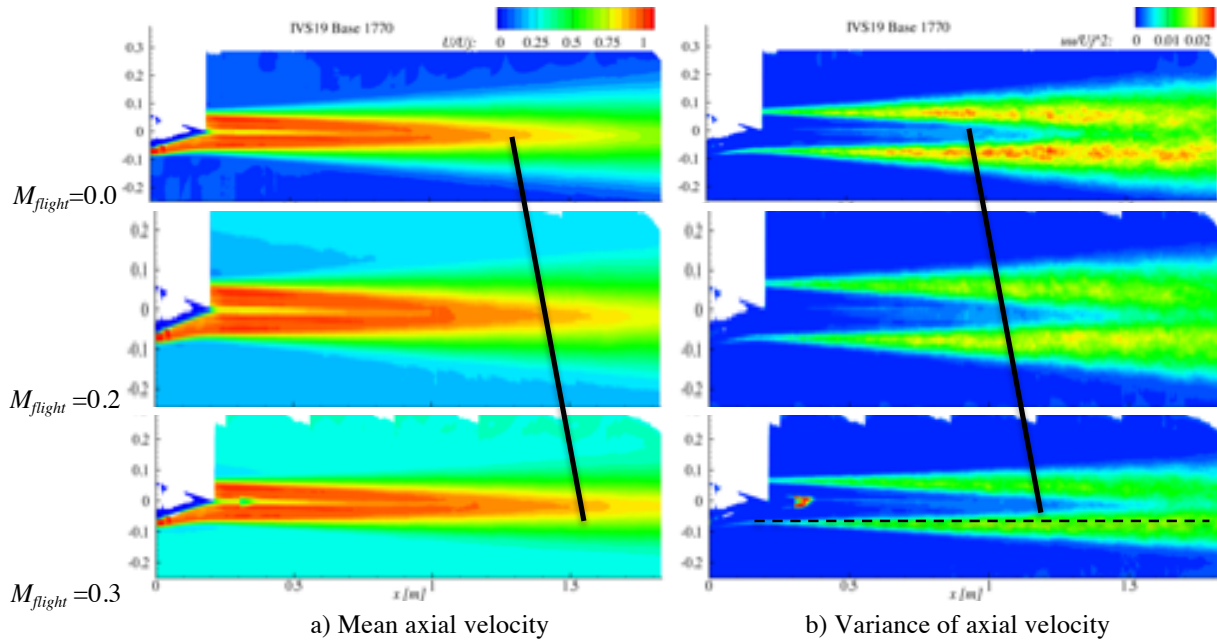
Figure 21 PIV measurements of mean and turbulent axial velocity for unheated, single-stream jet IV19 at Ma = 0.9, operating in different speed ambient flight streams. Solid lines drawn to note change in potential core length.
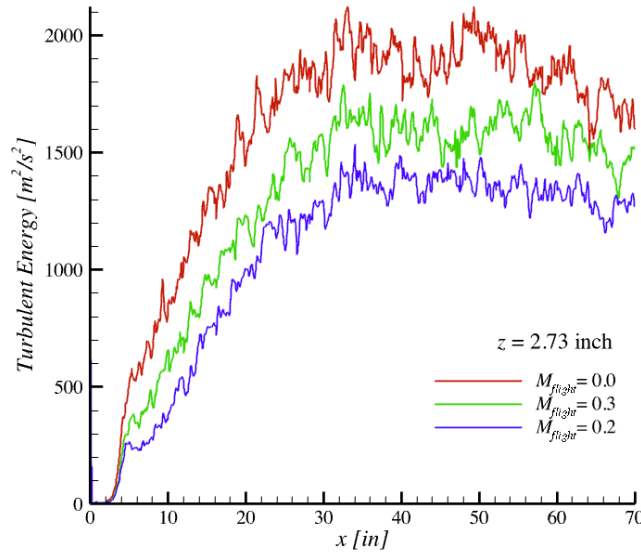
Figure 22 Turbulent energy in the shear layer (dashed line in Figure 21) for unheated, single-stream jet IV19 at Ma = 0.9, operating in different speed ambient flight streams.

3. *Impact of surface is not just acoustic shield*

If the aircraft planform had no impact on the jet plume and was strictly an acoustic shield, the source distributions measured with and without the planform downstream of its trailing edge would be the same. Region-of-interest (ROI) processing of the phased array data was used to look at source maps aft of the trailing edge location, with and without the Medium center-engine planform. Figure 23 and Figure 24 show the sound measured by the phased array for two configurations, one with and one without ('Bare') the planform, respectively. In each figure are three spatial source maps for one frequency and a plot of the spatially integrated power spectral density of each map. For the uninstalled, or 'Bare', configuration, two regions of interest are shown: the entire field of view and the portion downstream of where the planform trailing edge was in the installed case. The red line in the plot (corresponding to the red outline of the source map image) is the total sound of the uninstalled configuration, while the blue line shows
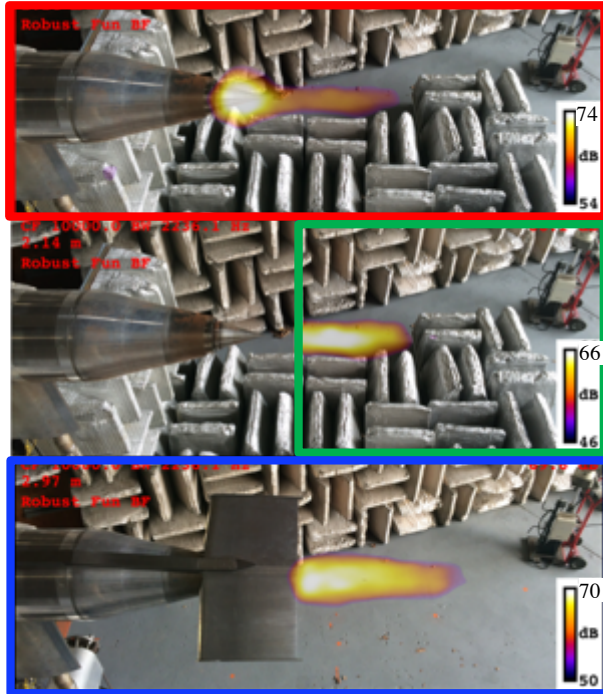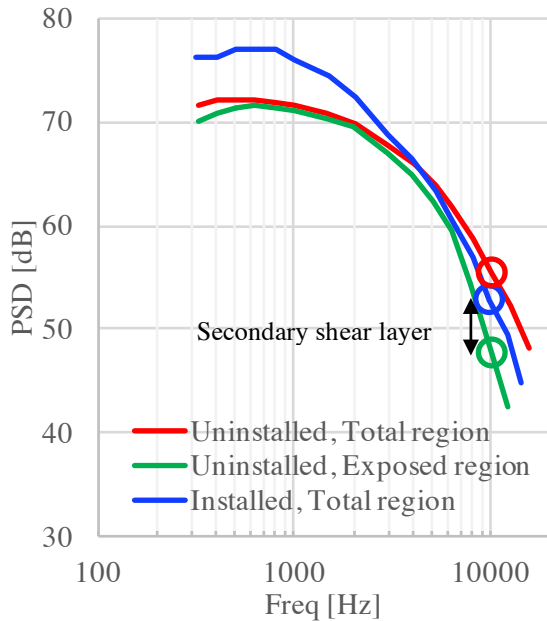
the sound of the uninstalled configuration that would not be shielded by the planform in the Med configuration. The black line shows the total sound of the installed configuration.

At low frequencies (Figure 23), sound sources are generally farther downstream than the length of the planforms used here, so there should be no shielding by the planform, and the installed and uninstalled would be the same. However, the sound of the installed configuration is greater than even the total sound of the uninstalled configuration. This is presumably because the addition of the planform creates a trailing edge dipole, as has been documented in far-field measurements[8].

At high frequencies (Figure 24), sound sources are generally located near the nozzle and the planform should provide some shielding of these. As expected, the sound of the uninstalled configuration is higher than the installed configuration. However, the high frequencies are not reduced as much as expected just by line-of-sight shielding. If the plume of the installed configuration had the same source distribution as the plume of the uninstalled configuration, and the planform only affected the propagation of sound, then the sound produced aft of the planform trailing edge would be the same in both configurations. Looking at the downstream portion of the uninstalled configuration allows direct comparison of the same portion of the plume in both the installed and uninstalled configuration (note the change in colorscales). Clearly, the noise produced by these two regions are not the same: the black and blue lines in the plot are not the same. The installed configuration is louder than expected. This could be due to noise refracting around the trailing edge, or it could be because the presence of the planform generates additional turbulence and mixing noise aft of planform. If the noise were from refracted sound, the source map of the installed case would show a strong 'source' at the trailing edge; however, this is not the case. The source maps show that the additional sound is produced well away from the trailing edge, supporting the conjecture that the planform is introducing a new shear layer, and hence new high frequency sources aft of the trailing edge.
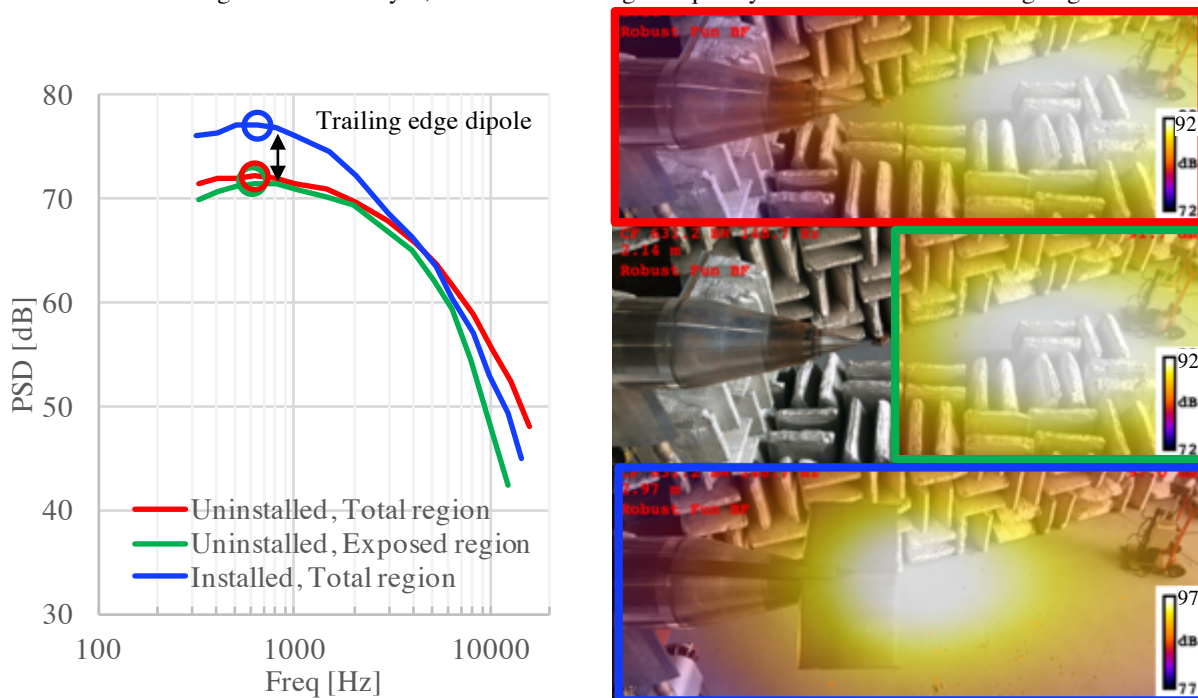
Figure 23 Phased array data for IV44, Bare and Medium planform. Processing using ROI to integrate sound from total uninstalled (red) and installed (blue) configurations, and from portion of uninstalled plume exposed in installed configuration (green). Source maps are for 600Hz, roughly the peak of the trailing edge dipole source.

Figure 24 Phased array data for IV44, Bare and Medium planform. Processing using ROI to integrate sound from total uninstalled (red) and installed (blue) configurations, and from portion of uninstalled plume exposed in installed configuration (green). Source maps are for 10kHz, representative of additional source from secondary shear layer produced by high speed flow on one side of planform.

D. Comparison of nozzle types (Objective 4a)

Recall that one of the main questions to be answered was whether there was an acoustic advantage to be obtained by directing a part of the tip fan stream around the outside of the primary stream (IV19), instead of diverting it all inside the primary stream (IV44). This had been addressed for isolated nozzles in the previous tests, and the noise found to have little change with how the tip flow was deployed. The question posed was whether installation would change this result. This might be caused by a difference in source distribution or by a change in local flow properties at the trailing edge of the planform. Here, we cursorily examine the difference in nozzle type for one fan pressure design, FPR=1.8 at 100% throttle point. The impact of the nozzle type and of the orientation of the buffer stream are considered separately.

4. Impact of nozzle type (IV44, IV19, and IV01)

Some sample spectral directivities of the three nozzle types being studied will be presented to give a feel for the differences in their spectral shapes. For the figures that follow, the nozzles were run on essentially the same engine conditions with design 100% throttle fan pressure ratio = 1.8, but the scale factors are not quite the same. All the plots show PSD at 1-foot, lossless condition in model scale. As a reminder, the IV01 nozzle only had a single hot stream from the primary nozzle, the IV44 had a cool inner stream ducted inside the primary stream, and the IV19 added a third outer stream around 180° of the primary stream.

For the spectral directivities shown in Figure 25, the nozzles are uninstalled (Bare). All nozzles exhibit some oscillations in the spectra at low frequency, independent of the polar angle. This was worse for the IV44 nozzle and no explanation has been found for this observation. The IV19 nozzle had significant oscillations in the spectra at high frequencies and forward-to-broadside angles. Notably, these oscillations vary with polar angle as well. This feature had been noted in earlier test programs with the 180° annular nozzle and seems to be a feature of the design. Two explanations have been put forth: (1) high frequency sources produced upstream in the outer shear layer reflected on the nozzle cowl and plug, producing interference effects in the spectra; or (2) the radial curvature of the flow over the cowl and plug produce weak shocks, and broadband shock noise is producing the high-frequency oscillations. The IV01 nozzle, which only has flow from the primary nozzle, produces spectra similar to the IV19, but without the oscillations that vary with polar angle.

In Figure 26, the same presentation style is used to show the spectral directivities for the nozzles when installed as the center engine with medium length planform. Now, none of the spectral directivities show high-frequency spectral oscillations. The IV44 has a slightly lower peak at the aft angles, and produces more low frequency noise at broadside angles than the IV19 and IV01. Thus, the IV44 nozzle could be described as producing a different directivity along the peak frequency.

Finally, in Figure 27, the nozzles are installed with the outboard planform, installed in the R60 position, and the spectral directivity of the nozzles again presented. Because the high frequency sources near the nozzle have been exposed, the anomalies at high frequency that were evident in the bare nozzles are again found in the data with the outboard planform.

In summary, there were small differences between nozzle types, most notably the high frequency oscillations in the spectra of the IV19 nozzle. This appears to be a feature of this nozzle type. In general, the difference in sound between the nozzles was mostly less than 3dB across the spectral directivity.

a) IV44 nozzle   b) IV19 nozzle   c) IV01 nozzle
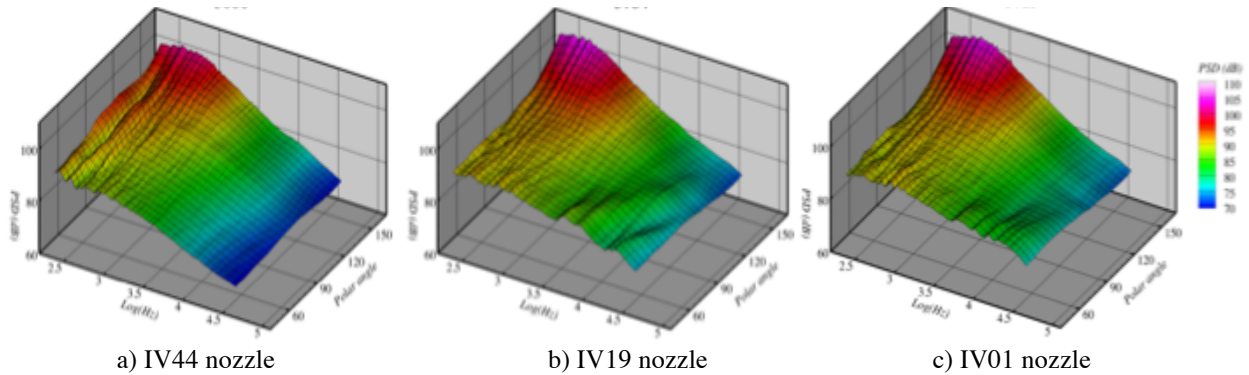
Figure 25 Spectral directivity of PSD for FPR1.8 engines at 100% throttle, uninstalled (Bare).

a) IV44 nozzle   b) IV19 nozzle   c) IV01 nozzle
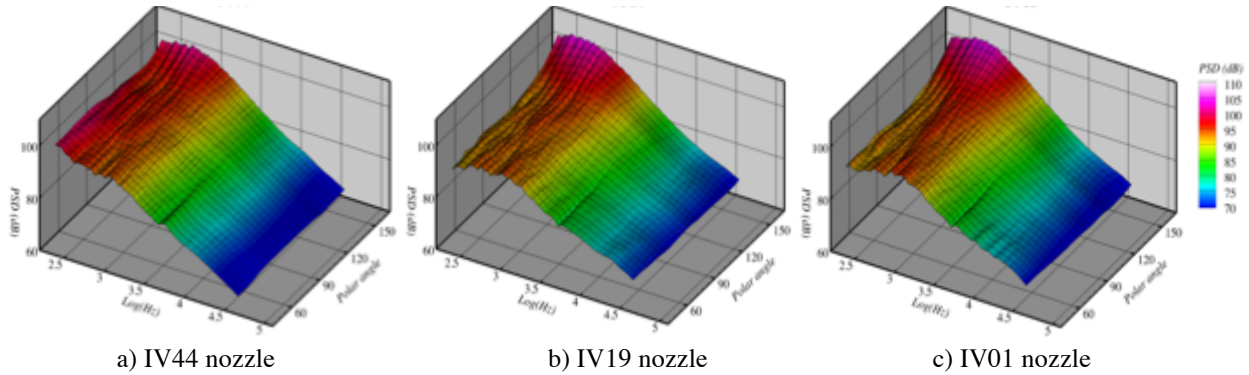
Figure 26 Spectral directivity of PSD for FPR1.8 engines at 100% throttle, installed on medium length center engine planform, flyover observer (S60).


a) IV44 nozzle   b) IV19 nozzle   c) IV01 nozzle
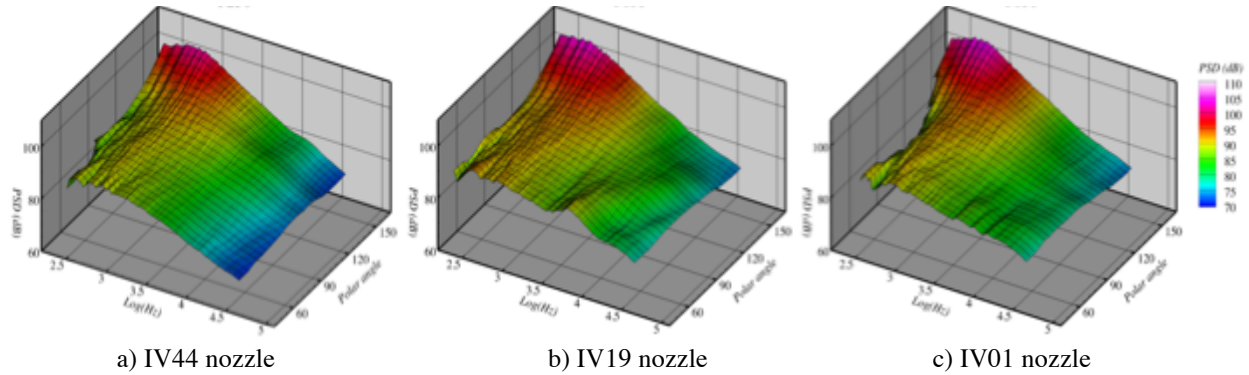
Figure 27 Spectral directivity of PSD for FPR1.8 engines at 100% throttle, installed on outboard engine planform, lateral observer (R60).

### E. Effect of planform length (Objective 4b)

Analysis of the effect of planform length is shown by considering the difference between the noise produced by a given nozzle planform and the noise produced by a bare nozzle. This is done for each type of nozzle (Figure 28–Figure 30) at the 100% throttle point on the FPR=1.8 engine design appropriate for that nozzle. In the case of the IV44 and IV19 nozzles, these are the same flow conditions, but with the tip flow being either totally directed to the inner stream or split 50/50 to the inner and buffer streams. However, there was a difference in linear scale factor (LSF) not represented in these figures. The IV44 had a LSF = 11.84 while the IV19 and IV01 had LSF = 14.0. Because the planform is the same size for all nozzles, the planform, in scale, was 18% bigger for the IV19 and IV01 nozzles.

a) Short planform   b) Medium planform   c) Long planform
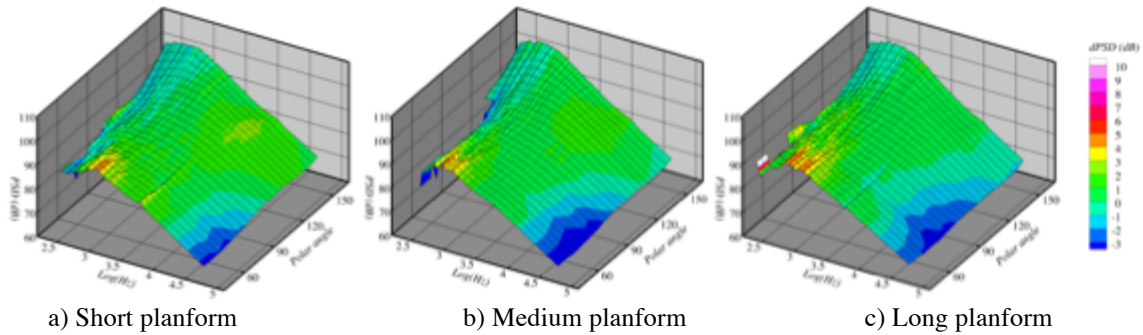
Figure 28 Spectral directivities of IV44 nozzle in center engine location at setpoint 255, seen by lateral observer (S60). Colors give delta over Bare configuration.

a) Short planform   b) Medium planform   c) Long planform
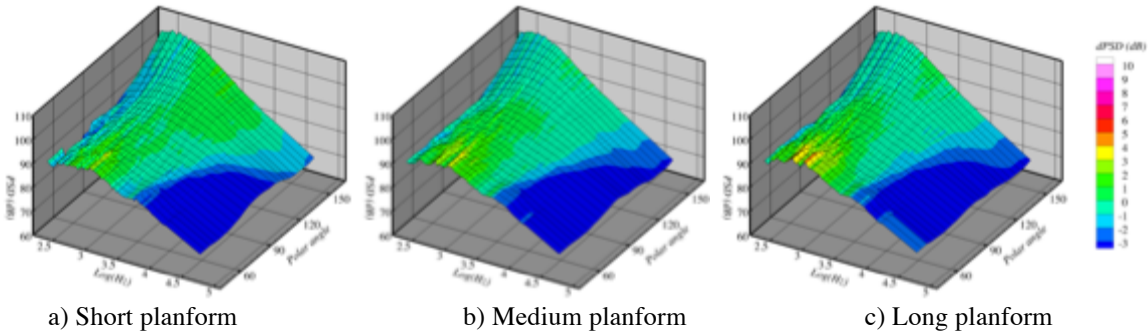
Figure 29 Spectral directivities of IV19 nozzle in center engine location at setpoint 155, seen by lateral observer (S60). Colors give delta over Bare configuration.

a) Short planform   b) Medium planform   c) Long planform
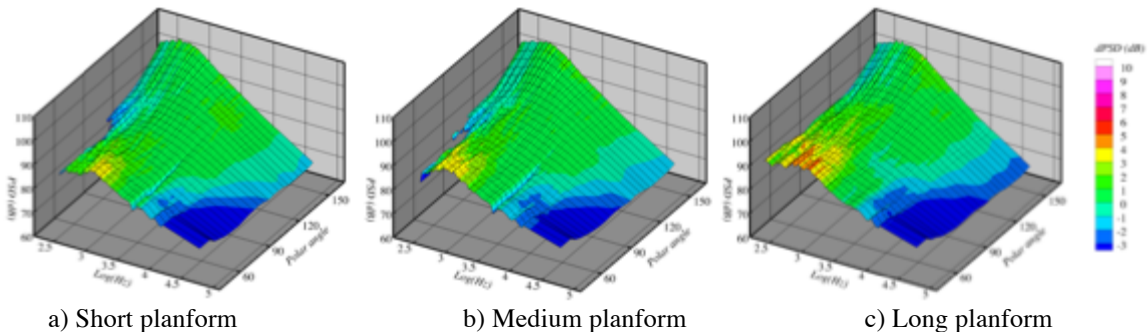
Figure 30 Spectral directivities of IV01 (MFTF) nozzle in center engine location at setpoint 355, seen by lateral observer (S60). Colors give delta over Bare configuration.

For all nozzles, there was an increase in noise with installation at the far forward angles (polar < 70°) associated with the trailing-edge dipole. There was a substantial decrease in noise with installation at the highest frequencies, weighted toward the forward angles, that comes from shielding the noise produced near the nozzle. For each nozzle, these two effects increase with planform length.

For the purposes of this test, which was validation of the acoustic performance of a conceptual vehicle design, it is more pertinent to consider the impact on EPNL. The impact on EPNL will depend upon where the cross-over

between low-frequency increase and high-frequency reduction landed relative to the critical 2.5kHz frequency band in full scale. EPNL were calculated for the four datasets available in this test where the length was changed for a given observer (S60). For this analysis, spectral directivity data were scaled to the same ideal thrust, and flown at the measured flight speed $M_{flight} = 0.3$.

First, consider Figure 31, with plots of EPNL for the IV44 nozzle with no planform (Bare), and short, medium and long planforms. Surprisingly, there was no EPNL benefit when the nozzle was installed with the short planform between the nozzle and observer. In fact, the short planform increased the EPNL for both engine cycles tested. Looking back at the spectral directivity plots for this nozzle (Figure 28), consider that the most significant frequency bands for EPNL is 2.5 kHz, which scales to 27.5 kHz in model scale. For these frequencies, the delta-PSD is slightly positive for most angles. This was true for both engine cycles tested.

The IVS19 nozzle (IV19 nozzle with the tip flow away from the planform), shown in Figure 32, showed a significant decrease in EPNL when installed, and a monotonic (but small) decrease with added length. The spectral directivities in Figure 29 do show a negative delta-dB with installation at the critical band, which is 35 kHz for this model. Similarly, the IV01 nozzle (Figure 33), representing a simple MFTF nozzle, showed a similar 2 EPNdB suppression with installation and a monotonic change with planform length (Figure 33).

a) EngineID 1648   b) EngineID 1672
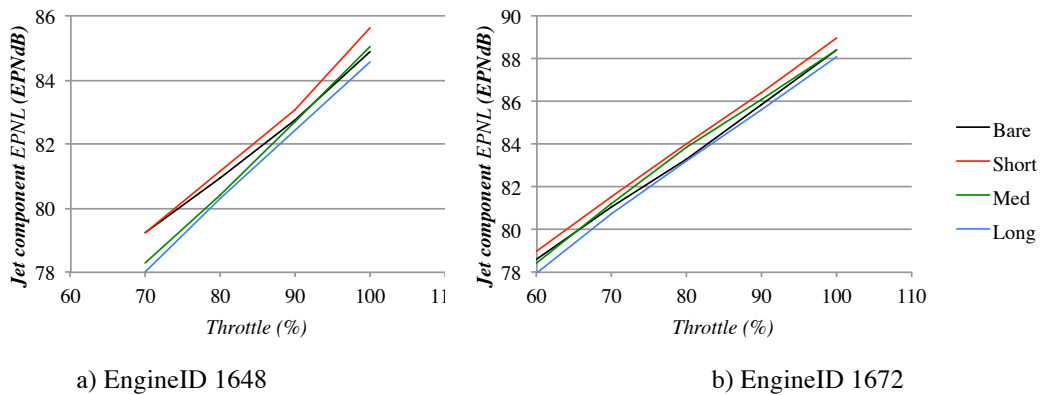
Figure 31 Lateral EPNL values over the throttle line for the IV44 center engine, varying the engine axial location (planform length).
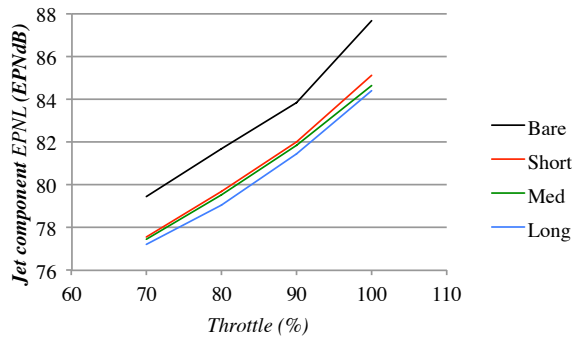
Figure 32 Lateral EPNL values over the throttle line for the IVS19 center engine, engineID 1549, varying the engine axial location (planform length).
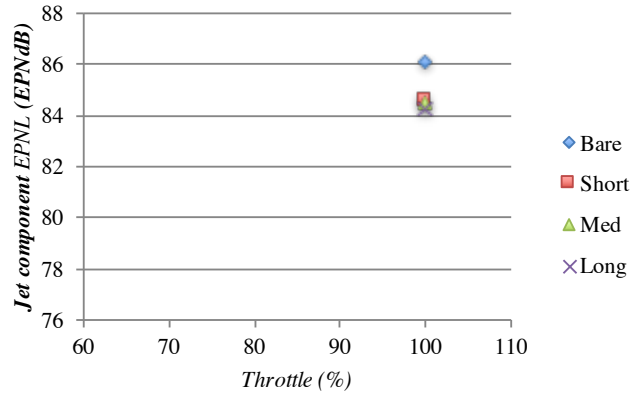
Figure 33 Lateral EPNL values for the IV01 center engine, engineID 2044 at full throttle, varying the engine axial location (planform length).

The outboard planform, not previously discussed, is a bit quieter than expected, its peak source amplitude being 1dB louder than the bare nozzle; a 3dB increase would have been expected for simple reflection, with some reduction for the fact that the planform is not a simple surface and only partially spans the jet plume.

The acoustic behavior of the installed IV44 nozzle is counter-intuitive. As a check, phased array source maps were acquired for the same configurations, and these measurements confirmed the far-field data. A cursory glance at the change in color scales in each image of Figure 34 shows how the bare nozzle is the loudest of all the center engine configurations at 6.3 kHz (model scale), which translates to roughly 600Hz fullscale. The medium length planform is the quietest.

PIV data, measuring the turbulence of the plumes with and without installation, give further insight. These are discussed below in Section H. The essence of the PIV data is that installation of the planform increased the TKE in the plume for the IV44 nozzle, but not for the IV19 or IV01 nozzles. The increased TKE produced stronger noise sources even as some of the sources were being covered by the planform.
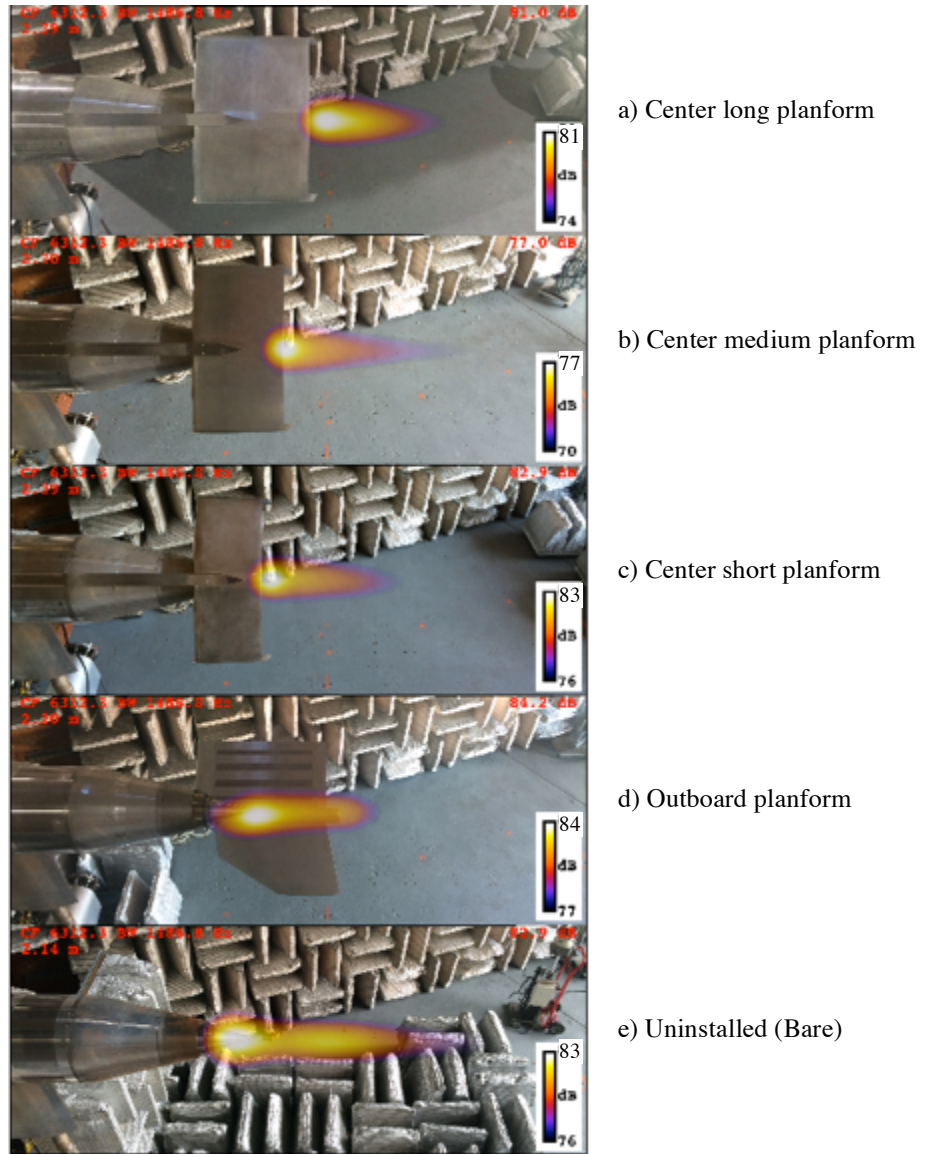
Figure 34 Source distributions at 6.3 kHz from phased array for IV44 nozzle, S0 observer angle, at set point 255 (100% throttle, M_{flight} = 0.3). Note the changes in amplitude (color bar) scale for each image.

F. Scaling with flight speed (Objective 4c)

Because the *LM1044* concept aircraft was designed to be flown fast over the acoustic certification observer (M_{flight}=0.38) and NATR could not consistently achieve this speed with a low enough background noise level, extrapolation of data from lower flight speeds was required. This was done using the flight effect exponent construct. Viswanathan & Czech[15] (hereafter VishyCzech) provide background information.

Flight effect is classically captured by flight exponent k to relate the noise (PSD) at two flight speeds, $V_{\infty,1}$ and $V_{\infty,2}$:

$$\text{PSD}(V_{\infty,1}) + k * 10 \log_{10}(V_j - V_{\infty,1}) = \text{PSD}(V_{\infty,2}) + k * 10 \log_{10}(V_j - V_{\infty,2}) \qquad [1]$$

where V_j is the jet velocity. V_j is somewhat arbitrarily defined for an externally mixed jet, but the fully-mixed jet velocity was used in this analysis.

In principle, since PSD is frequency- and angle-dependent, k should be as well. Some models, such as VishyCzech, ignore the frequency dependence, effectively creating a flight effect for OASPL as a function of observer angle, and some have simply applied a global exponent, essentially correcting the OAPWL.

In the present analysis, a value for k was found from Eq [1] for each flight speed using the PSD at the flight speed and the PSD at zero flight speed. These k values were insensitive to the flight speed and to the throttle settings for any given nozzle. In fact, the results were relatively insensitive to the installation as well. The values for k were averaged over flight speed and throttle setting to create a 'universal' k factor that could be applied to all engine cases. The result of this exercise is shown in Figure 35 for two nozzles, IV44 and IVS19. Note that there are some differences between the two nozzles at high frequencies in aft directions as the IV44 has a spectral characteristic that the IVS19 does not. This spectral characteristic is more sensitive to flight speed than most sources at this angle/frequency.

| a) IV44 nozzle | b) IV19 nozzle |
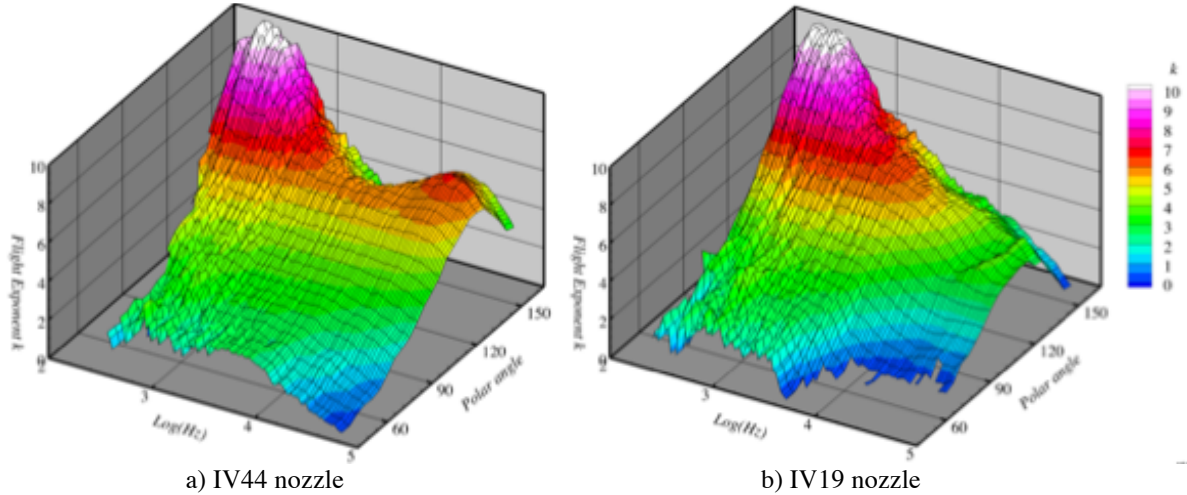
Figure 35 Flight exponent k as a function of frequency and polar angle, computed by averaging values found from flight speeds $0.25 < M_{flight} < 0.35$ and four throttle points.

The flight exponent for installed jets was similar to the uninstalled jets, except at high frequencies. Figure 36 shows the flight exponent as a function of frequency and polar angle (spectral directivity) for the uninstalled (Bare) nozzle and when the medium planform was installed for an observer on the symmetry plane (S0). In both cases the flight exponent is relatively constant, 3-5, over the broadside angles, but peaks sharply to 10 at the aft angles and low frequencies. There are clearly differences in the spectral directivity of k when the planform is installed, but a direct subtraction of the two cases, given in Figure 37, makes it even clearer.


| a) Isolated IV01 nozzle | b) IV01 nozzle on medium planform |
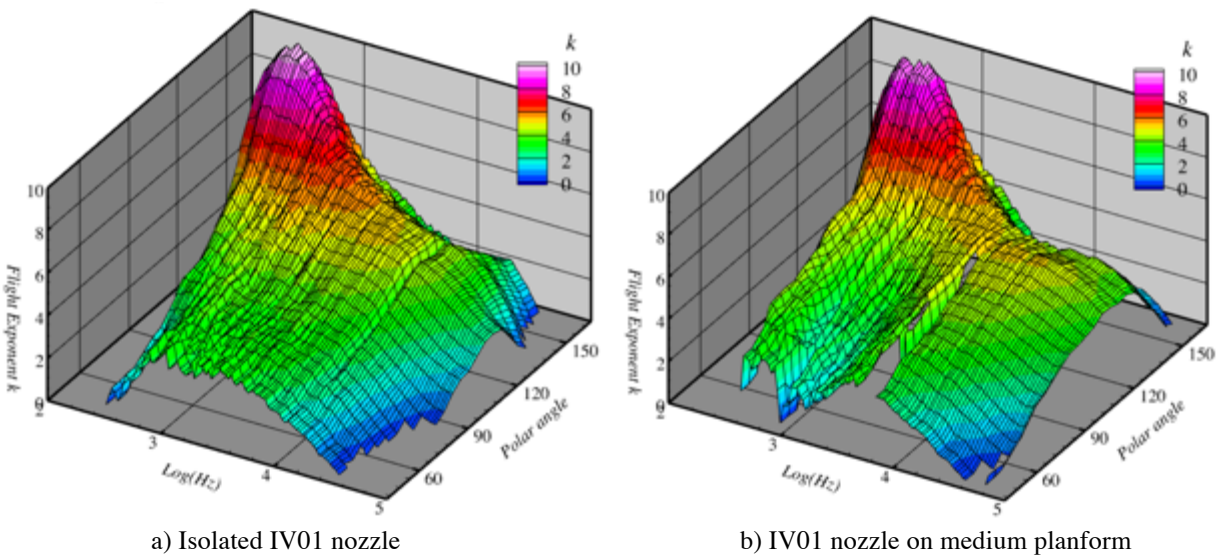
Figure 36 Spectral directivity of flight exponent k derived from single-stream Ma=0.9, unheated jet flow in different flight stream speeds.

At the peak jet mixing noise frequencies at aft angles (which coincides with the peak values of k) the difference in k, installed vs uninstalled, was small, less than 1. However, at higher frequencies and broadside angles the difference in k was much greater, with k increasing from ~2 to ~4 when the planform was installed. This means that the flight

effect for installed configurations was more significant than for uninstalled configurations. Recall that sources very near the nozzle lip were less sensitive to the flight stream (Figure 20), making the flight exponent smaller at high frequencies for the uninstalled nozzles. With the planform in place, the sources not shielded were more affected by the flight stream.

Figure 37 also shows a significant difference over broadside angles at lower frequencies, here around 1 kHz, where the difference was negative because the exponent is smaller when the nozzle was installed. This frequency seems to coincide with the trailing edge dipole, indicating that the JSI trailing edge dipole probably had less change with flight speed than the jet mixing noise sources.
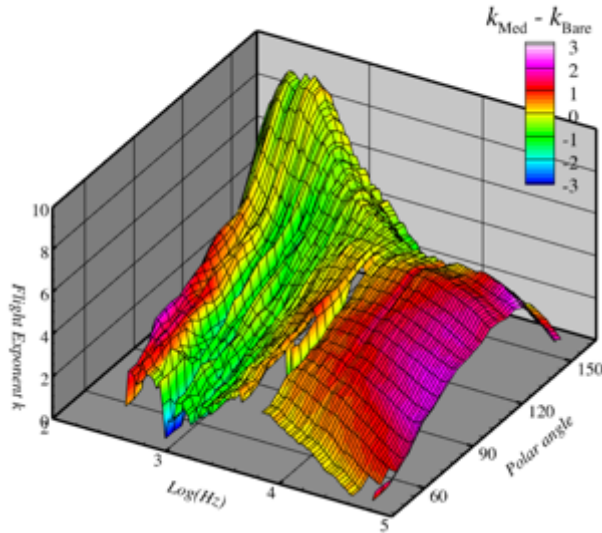

Figure 37 Spectral directivity of differences in flight exponent k for bare nozzle and installed on medium planform (see Figure 36). Surface shape given by k for nozzle installed on medium planform, color scales relate difference in k value, k$_{med}$ – k$_{bare}$, with installation.

The flight exponent *k* is a strong factor in both frequency and polar angle. VishyCzech document a model for *k* as a function of polar angle only. This was compared against current findings by averaging the *k* values found in the current test data over frequency. These values, k_{bar}, are shown plotted along with the VishyCzech model in Figure 38 for the IV44 nozzle. In these plots, the VishyCzech model passes through the data and has the advantages of being documented and very simple to express. Therefore, although *k* is a very strong factor of frequency in the data, the VishyCzech model was used in extrapolating the data for evaluation of the data at higher flight speeds. Furthermore, as was discussed in section *C*, the flight effect of the installed nozzle did not exhibit as much variation with frequency at the high frequencies as that of the uninstalled nozzle, making this assumption better for the installed cases being studied here.
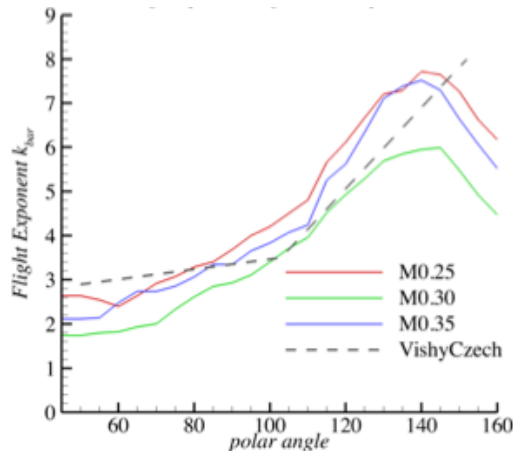
Figure 38 Flight exponent k$_{bar}$ (average over frequency) as a function of polar angle, as determined by several flight speeds and compared with literature reference.

As a final check on the extrapolation method, data acquired at one flight speed were extrapolated using the VishyCzech model and compared with data acquired at the extrapolated flight speed. This was done for two flight speeds, $M_{flight} = 0.25$ extrapolated to $M_{flight} = 0.3$, $M_{flight} = 0.3$ to M_{flight} to 0.35. For completeness, the $M_{flight} = 0.35$ was also extrapolated to $M_{flight} = 0.38$ to show that the last extrapolation is not very extreme and there is a high degree of confidence in this step. The comparisons were made in EPNL for the installed configuration of the IV44 Med (S0), shown in Figure 39. The error at each step (extrapolating by $\Delta M_{flight} = 0.05$) is less than 0.1 EPNdB. This validates the test methodology of acquiring data at $M_{flight} = 0.3$ and extrapolating to nearby speeds as design requirements change using the VishyCzech model.
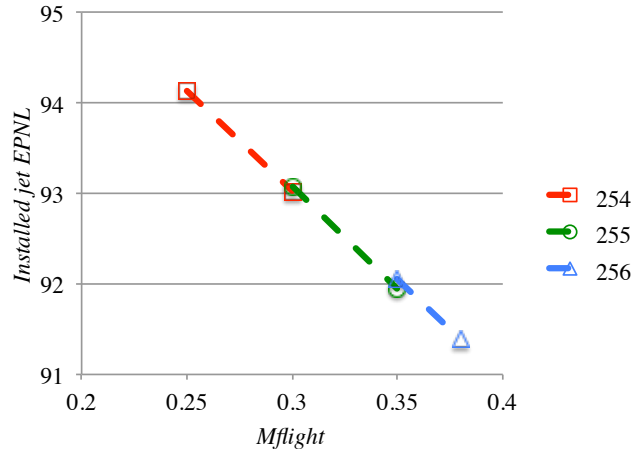
Figure 39 Demonstration of extrapolating data in flight speed using VishyCzech model. IV44 Med (S0) configuration at setpoints 25x.

In summary, the flight exponent model of VishyCzech was found to be adequate for scaling of data to different flight speeds in this application, with an accuracy as good as the test data (0.1EPNdB). Although the model does not include spectral dependence, and there was significant spectral dependence found in the data, the VishyCzech model matched the data at frequencies which impact the annoyance the most for this application. In addition, as shown in Section *C*, the sources that were created or modified by the presence of the installed planform were adequately addressed by the VishyCzech model so that the model can be used on installed configurations as well.

G. Effect of top/bottom engine location and azimuthal sensitivity (Objective 4d)

Usually, suppressions of jet mixing noise focus on reducing the source strength. Since jet noise is produced over a relatively long region of the jet plume, that is not easily contained. Little effort has gone into reduction-by-obstruction in conventional tube-and-wing aircraft. In the LM1044 aircraft there is substantial room for noise from the plume to either be shielded or reflected. The center engine is located roughly 3 nozzle diameters upstream of the aft deck trailing edge, while the sponsons and aft deck extend almost 5 diameters downstream of the outboard engine nozzles. There is also interest in moving the engines, which are mounted aft on supersonic aircraft, above the wing to avoid debris being thrown in the engine inlet from the tires. Accounting for the impact of the airframe surface on the exhaust noise is critical. It is also critical to know whether modifications to the plume, such as the 180° buffer flow, can make a difference in how the plume and planform interact and make noise. In this section, the exhaust noise of the engine mounted on top and underneath are directly compared.

Starting with spectral directivities, the PSD from the three nozzle types mounted underneath and on top is directly compared in Figure 40. In the figure, the color contours are the difference in PSD between the top-mounted, center engine installation and the underneath, outboard engine installation. The engine cycles were ones that met the Tech Challenge noise goal operating at 100% throttle (fan pressure ratio = 1.8 designs) and all measurements were made in the lateral observer direction. As expected, the noise from the top-mounted engine was lower than from the underneath engine, with the exception of a small increase at low frequencies and angles associated with the trailing edge dipole. Certainly, the high frequencies experienced a very strong reduction from the shield of the planform. Over the broadside angles, the reduction was anywhere from 5 to 10dB. The least difference was for the IV44 nozzle. The IV19 nozzle had a broad range of frequencies that were impacted, possibly because that nozzle exhibited broadband (not just high frequency) noise sources near the nozzle.
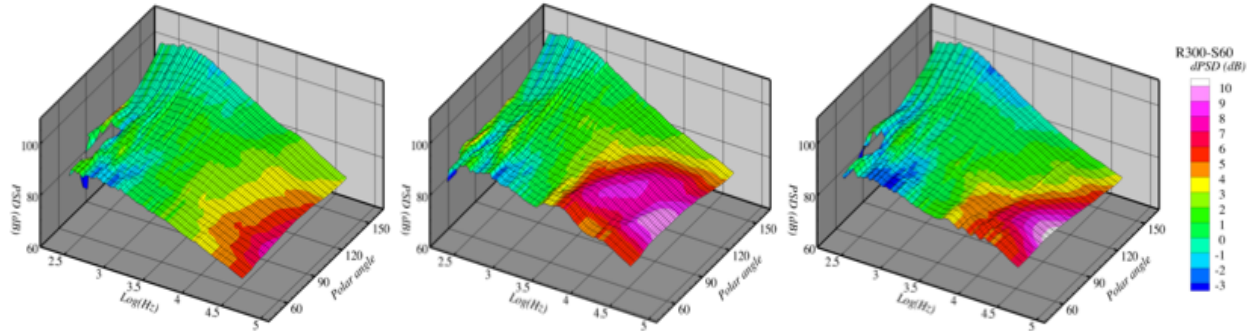
a) IV44, long planform   b) IV19, long planform   c) IV01, long planform

Figure 40 Spectral directivity of PSD for three nozzles when mounted underbody and overbody. Surface shape is from engine mounted underbody (R300), surface color is difference between overbody (S60) and underbody mounting (positive means underbody is louder).

Figure 41 gives the EPNLs calculated from the individual configurations, including both near- and far-side engines for the outboard configuration. For each engine in the plots, there was a significant difference due to the installation. The IV44 nozzle had the least difference, with a consistent 2 EPNdB difference over the throttle line. The IV19 had 4-6 EPNdB difference until the highest throttle of the FPR=2.0 engine when the difference becomes 2-3 EPNdB. The IV01 nozzle, running as a single-stream, internally mixed nozzle, produced 3 EPNdB difference with installation. Based on this small sampling the nozzles that have external mixing streams were most impacted by installation, presumably because they had the most noise sources near the nozzle.
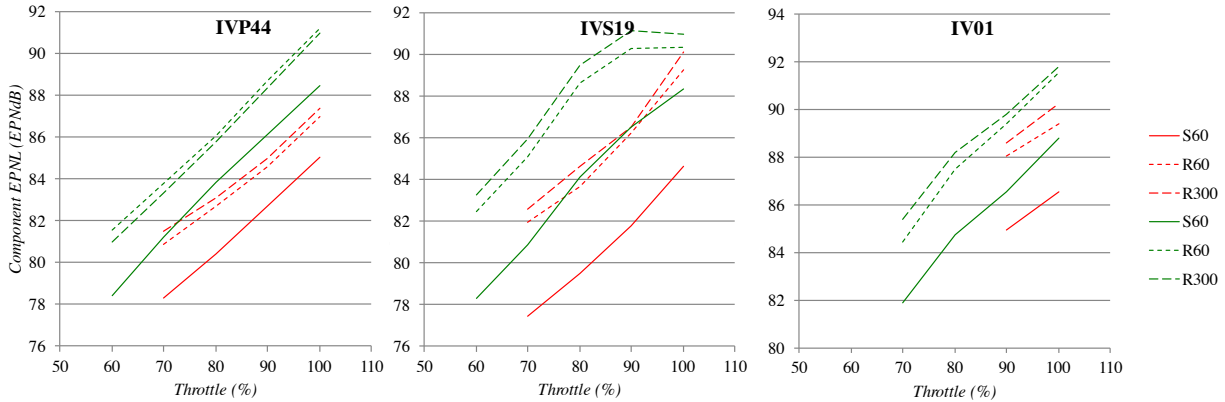

a) IV44 nozzle   b) IV19 nozzle   c) IV01 nozzle

Figure 41 Component lateral EPNL for test nozzles installed over aft deck (center engine, medium planform, S60), and underbody (outboard engines, R60 and R300). Nozzles and planform rotations are identified on plots, Red lines are FPR=1.8 engine cycles, green for FPR=2.0 engine cycles.

H. Document impact of surface on jet plume for CFD validation (Objective 5)

As alluded to above, the effect of installation is not just that of an acoustic barrier to sound; the presence of the surface downstream of the nozzle often distorts the plume and can create a new secondary shear layer at the trailing edge of the surface. To document the impacts of the installation on the plume in this test, PIV data were acquired on the streamwise plane normal to the pylon and in cross-stream planes down the plume. Figure 42 shows a representative depiction of the measurement regions, showing the mean velocity of the IV44 nozzle with the short center-engine planform. One feature notable from this figure was the narrow extension on the top of the cross-section from where the flow attached to the pylon. This feature sets up counter-rotating vortices and induces turbulence in the installed configurations.
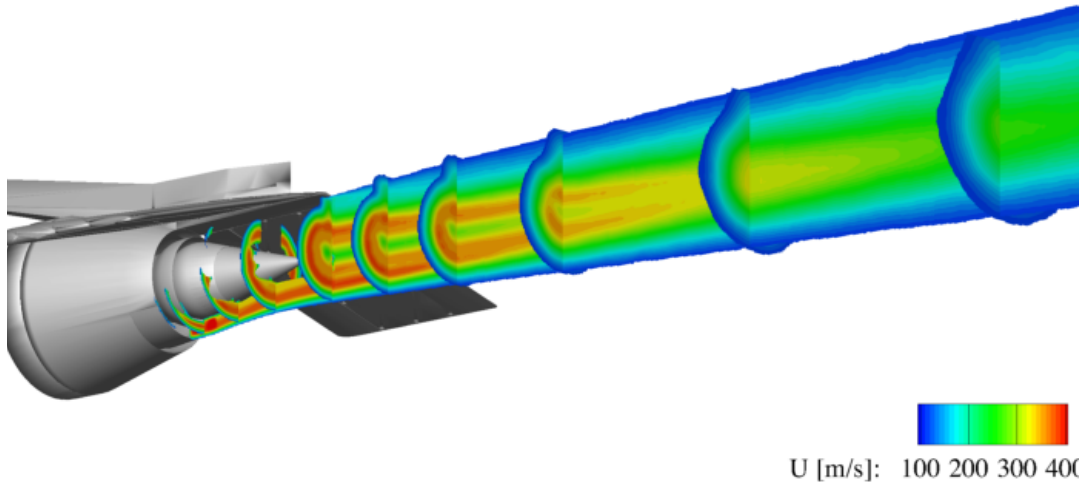
Figure 42 Mean axial velocity of the IV44 nozzle at setpoint 255, measured with PIV. Contours blanked for velocities of the flight stream and below.

Figure 43 shows cross-sections of the turbulent kinetic energy (TKE) for the IV44 nozzle at setpoint 255, uninstalled and with the three different planform lengths for the center engine. For clarity, the contours have been blanked for values of TKE < 300 m^2/s^2. All installed plumes showed an outward bump in the shear layer on the top of the plume where the high-speed flow attached to the underside of the pylon. The TKE in the installed cases was generally greater than in the uninstalled case. As the planform length increased, the portion of the plume covered by the surface increased, but the TKE at the downstream-most cross-section shown here remained the same, being higher than the uninstalled case. Recall that the noise of the IV44 nozzle increased when the short planform was installed, and after the initial increase in noise with installation of the short planform, the noise decreased with increasing length of the planform. Here, the TKE is shown to increase with the installation of the short planform and then remain relatively unchanged with planform length, possibly explaining the acoustic observations.

a) Uninstalled

b) Short planform

c) Medium planform

d) Long planform
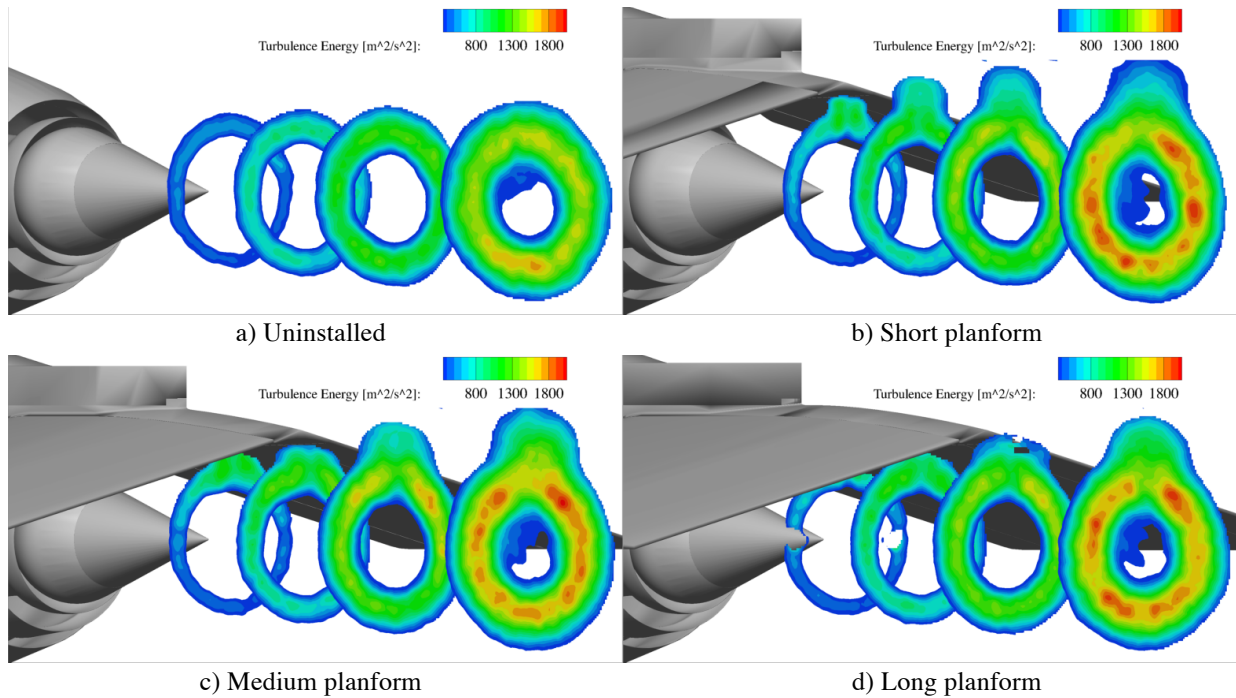
Figure 43 Turbulent Energy in cross-stream planes. IV44 at setpoint 255, uninstalled and installed on different length planforms.

The same presentation of TKE is made for the IVS19 nozzle (tertiary nozzle opposite planform) at setpoint 155 in Figure 44. In this set of plots, there was not the same increase of TKE with installation as in the IV44 case above. There still is the extracted tongue of the plume by the pylon. But, within the uncertainty of the measurements the TKE in corresponding cross-sections was the same between all configurations of the IVS19 nozzle. This correlates with the reduction in sound for all lengths of planforms. There was little modification in the TKE levels with the installation of the planform on the IVS19 nozzle.

a) Uninstalled	b) Short planform

c) Medium planform	d) Long planform
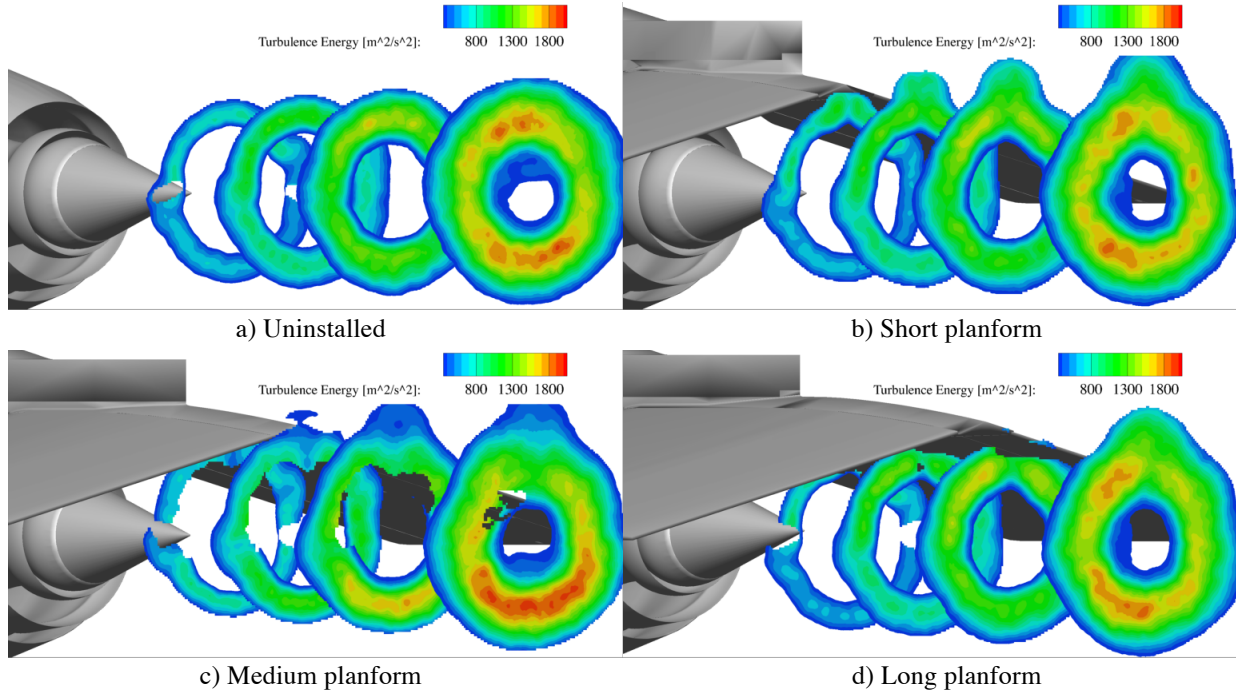
Figure 44 Turbulent Energy in cross-stream planes. IVS19 at setpoint 155 , uninstalled and installed on different length planforms.

The flow field of the IV01 nozzle was only measured uninstalled and with the medium length planform. Figure 45 presents those TKE cross-sections. The planform again produced an extension in the cross-section where the flow attached to the pylon. The TKE amplitude was not significantly changed by the installation of the planform. This again correlates to the observed acoustic impact of installation, where the installation always produced reduction in noise.

a) Uninstalled	b) Medium planform
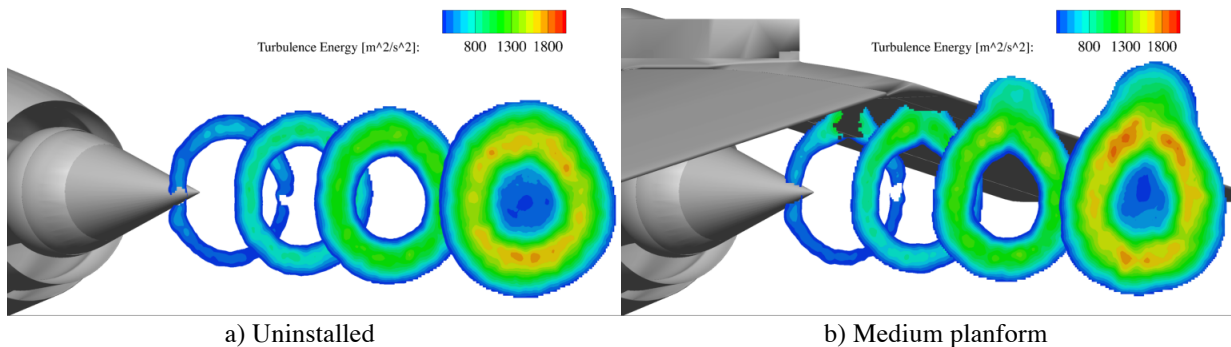
Figure 45 Turbulent Energy in cross-stream planes. IV01 at setpoint 355 uninstalled and with medium center-engine planforms.

VIII.   Summary

A system-level engine/nozzle design exercise produced a set of designs that met the Commercial Supersonic Project's Technical Challenge goal for propulsion exhaust noise for a conceptual supersonic airliner, the LM1044. Most of these designs featured a three-stream, variable cycle engine. The acoustic performance of these designs was validated in a test campaign called *JSI16* (*Jet-Surface Interaction Test 2016*). Three nozzle types were tested for

several engine cycles. Two of the nozzle types were applied to variable cycle engines (VCE). These assumed that the core and bypass fan flows were internally mixed while the tip fan flow was either (1) redirected to the center of the engine to make an inverted velocity profile plume, or (2) split, with the flow directed half to in inner and half to the outer annulus. In addition, a conventional MFTF engine design was tested that did not have a tip fan flow and resulted in a warm single-stream plume.

The nozzles were tested both in isolation and with a planform representation of the concept LM1044 aircraft for the center engine and outboard engine installations. Far-field acoustic measurements were processed to simulate the sound of the aircraft flying past the lateral certification observer according to FAA/ICAO procedures. An acoustic phased array was used to validate several key assumptions regarding the representation of the aircraft by the planform model, and to provide insight for further improvements in the designs. PIV was also deployed to validate that the flows around the nozzle were representative of those to be found around the nacelle and nozzle of the *LM1044*. PIV data will allow validation of computer simulations of the jet plumes to be used in future noise predictions. This paper summarizes the configurations, flows, and key findings of the test. It also documents the efforts made to establish the validity of these measurements and their imperfections. The report specifically addresses the steps taken to meet the test objectives, including verifying that the designs did meet the expected project noise goal.

As part of the test, the impact of flight on the jet mixing noise was measured for uninstalled and installed jets. The data was analyzed in the context of a flight exponent. Although the flight exponent was frequency-dependent, previously documented frequency-independent models did a good job of fitting the data, both for installed and uninstalled jets. One puzzle was found when looking at the effect of flight on noise source distributions measured with a phased array: the source distributions did not seem to elongate downstream with flight speed even though PIV found that the plume did. This is important to understand if jet noise shielding is to be used as a noise reduction mechanism.

The aeroacoustic impacts of installation on the exhaust noise could be viewed as two types of effects: changes in the flow, and hence source strengths, and changes in the acoustic propagation of noise to far-field observers, either reflection or shielding. Overall, the presence of the planforms did not radically change the structure of the plumes in these geometries. A small modification of the plume cross-section was noted in all the configurations, where a narrow piece of high speed fluid hugged the pylon. The pure inverted velocity profile nozzle exhibited amplified turbulence for all planforms, regardless of length. This produced more high-frequency noise, countering the noise reduction produced by shielding some of the plume. All the nozzles exhibited a trailing-edge dipole from the turbulence in the plume interacting with the edge of the planform, which increased in strength with increasing planform length, but the amplitude did not appear to be the same for all nozzles. Accounting for the changes in turbulence level caused by the installation of the planform, the acoustic shielding was roughly what was expected, with those high frequency sources identified by the phased array as being produced near the nozzle being most attenuated by the planform. In most cases the top-mounted engine installations produced 3-4 EPNdB less noise than the engines installed under the aircraft, showing the attraction of mounting propulsion nozzles on the top of future vehicles.

Acknowledgements

References

[1] Bridges, J., Brown, C. A., and Seidel, J. A., "NASA's Pursuit of Low-Noise Propulsion for Low-Boom Commercial Supersonic Vehicles," *54th AIAA Aerospace Sciences Meeting*, 2018.

[2] Bridges, J. E., Podboy, G. G., and Brown, C. A., "Testing Installed Propulsion For Shielded Exhaust Configurations," *22nd AIAA/CEAS Aeroacoustics Conference*, American Institute of Aeronautics and Astronautics, 2016.

[3] Brown, C. A., "Including Finite Surface Span Effects in Empirical Jet-Surface Interaction Noise Models," *54th AIAA Aerospace Sciences Meeting*, American Institute of Aeronautics and Astronautics, 2016.

4   Brown, C. A., Podboy, G. G., and Bridges, J. E., "Modeling Jet-Surface Interaction Noise for Separate Flow Nozzles," *22nd AIAA/CEAS Aeroacoustics Conference*, American Institute of Aeronautics and Astronautics, 2016.

5   Huff, D. L., Henderson, B. S., Berton, J. J., and Seidel, J. A., "Perceived Noise Analysis for Offset Jets Applied to Commercial Supersonic Aircraft," *54th AIAA Aerospace Sciences Meeting*, American Institute of Aeronautics and Astronautics, 2016.

6   Morgenstern, J., Buonanno, M., Yao, J., Murugappan, M., Paliath, U., Cheung, L., Malcevic, I., Ramakrishnan, K., Pastouchenko, N., Wood, T., Martens, S., Viars, P., Tersmette, T., Lee, J., Simmons, R., Plybon, D., Alonso, J., Palacios, F., Lukaczyk, T., and Carrier, G., *Advanced Concept Studies for Supersonic Commercial Transports Entering Service in the 2018-2020 Period Phase 2*, 2015.

7   Tanna, H. K., Dean, P. D., and Burrin, R. H., *The Generation and Radiation of Supersonic Jet Noise. Volume 3. Turbulent Mixing Noise Data*, LOCKHEED-GEORGIA CO MARIETTA, LOCKHEED-GEORGIA CO MARIETTA, 1976.

8   Brown, C. A., "Jet-Surface Interaction Test: Far-Field Noise Results," *Journal of Engineering for Gas Turbines and Power*, vol. 135, Jun. 2013, pp. 071201-071201-7.

9   Brown, C. A., "Empirical Models for the Shielding and Reflection of Jet Mixing Noise by a Surface," *21st AIAA/CEAS Aeroacoustics Conference*, American Institute of Aeronautics and Astronautics, 2015.

10   Bridges, J., and Wernet, M., "PIV Measurements of Supersonic Internally-Mixed Dual-Stream Jets," *17th AIAA/CEAS Aeroacoustics Conference (32nd AIAA Aeroacoustics Conference)*, American Institute of Aeronautics and Astronautics, 2011.

11   Henderson, B., and Wernet, M., "An experimental investigation of overexpanded jets with chevrons," *Journal of Sound and Vibration*, vol. 351, Sep. 2015, pp. 119–142.

12   Brown, C. A., and Wernet, M. P., "Jet-Surface Interaction Test: Flow Measurement Results," *20th AIAA/CEAS Aeroacoustics Conference*, American Institute of Aeronautics and Astronautics, 2014.

13   Brown, Clifford A., "Evaluating the Assumptions in an Empirical Jet-Surface Interaction Noise Model," *AIAA SciTech Conference*, 2018.

14   Bridges, J. E., "Simple Scaling Of Multi-Stream Jet Plumes For Aeroacoustic Modeling," *54th AIAA Aerospace Sciences Meeting*, American Institute of Aeronautics and Astronautics, 2016.

15   Viswanathan, K., and Czech, M. J., "Measurement and Modeling of Effect of Forward Flight on Jet Noise," *AIAA Journal*, vol. 49, 2011, pp. 216–234.